Published in final edited form as:

Immunity. 2019 November 19; 51(5): 885–898.e7. doi:10.1016/j.immuni.2019.08.011.

MHC class II antigen presentation by the intestinal epithelium initiates graft-versus-host disease and is influenced by the microbiota

Motoko Koyama[1,15,*], **Pamela Mukhopadhyay**[2], **Iona S Schuster**[3,4,5], **Andrea S Henden**[1,6], **Jan Hülsdünker**[7,8,9], **Antiopi Varelias**[1], **Marie Vetizou**[10], **Rachel D Kuns**[1], **Renee J Robb**[1], **Ping Zhang**[1], **Bruce R Blazar**[11], **Ranjeny Thomas**[12], **Jakob Begun**[13], **Nicola Waddell**[2], **Giorgio Trinchieri**[10], **Robert Zeiser**[7], **Andrew D Clouston**[14], **Mariapia A Degli-Esposti**[3,4,5], **Geoffrey R Hill**[1,6,15,16,17,*]

[1]Bone Marrow Transplantation Laboratory, Immunology Department, QIMR Berghofer Medical Research Institute, Brisbane, QLD 4006, Australia

[2]Medical Genomics Laboratory, Genetics and Computational Biology Department, QIMR Berghofer Medical Research Institute, Brisbane, QLD 4006, Australia

[3]Immunology and Virology Program, Centre for Ophthalmology and Visual Science, The University of Western Australia, Crawley, WA 6009, Australia

[4]Centre for Experimental Immunology, Lions Eye Institute, Nedlands, WA 6009, Australia

[5]Infection and Immunity Program and Department of Microbiology, Biomedicine Discovery Institute, Monash University, Clayton, VIC 3800, Australia

[6]Department of Haematology and Bone Marrow Transplantation, Cancer Care Services, Royal Brisbane and Women's Hospital, Brisbane, QLD 4029, Australia

[7]Department of Hematology, Oncology and Stem Cell Transplantation, Freiburg University Medical Center, Albert Ludwigs University Freiburg, Freiburg 79106, Germany

[8]Spemann Graduate School of Biology and Medicine, University Freiburg, Freiburg 79085, Germany

[9]Faculty of Biology, University Freiburg, Freiburg 79104, Germany

[*]Corresponding authors: Motoko Koyama, MD, PhD, Fred Hutchinson Cancer, Research Center, 1100 Fairview Ave N, Seattle, WA 98109, USA, mkoyama@fredhutch.org, Phone: +1 206-667-2769; Geoffrey R Hill, MD, Fred Hutchinson Cancer Research Center, 1100 Fairview Ave N, Seattle, WA 98109, USA, grhill@fredhutch.org, Phone: +1 206-667-3324.

Author contributions

M.K. designed, performed and analyzed the majority of experiments and wrote the paper. P.M. performed the bioinformatics analysis. I.S.S., A.V., P.Z. helped design experiments. I.S.S., A.S.H., J.H., M.V., R.D.K., R.J.R. performed research. J.H., A.D.C. performed the histological analysis. B.B.B, R.T., J.B., N.W., G.T., R.Z., A.D.C. provided data interpretation. M.A.D-E. helped design experiments and wrote the paper. G.R.H. designed experiments and wrote the paper. Results were discussed and the manuscript was critically commented on and edited by all authors.

Declaration of Interests

The authors declare no competing financial interests.

[10]Cancer and Inflammation Program, Center for Cancer Research, NCI, NIH, Bethesda, MD 20892, USA

[11]Division of Blood and Marrow Transplantation, Department of Pediatrics, University of Minnesota, Minneapolis, MN 55455, USA.

[12]Diamantina Institute, Translational Research Institute, University of Queensland, Princess Alexandra Hospital, Brisbane, QLD 4102, Australia.

[13]Mater Research Institute, University of Queensland, Translational Research Institute, Brisbane, QLD 4102, Australia

[14]Envoi Specialist Pathologists, Brisbane, QLD 4006, Australia

[15]Clinical Research Division, Fred Hutchinson Cancer Research Center, Seattle, WA, 98109, USA

[16]Division of Medical Oncology, University of Washington, Seattle, WA, 98109, USA

[17]Lead Contact

Summary

Graft-versus-host disease (GVHD) in the gastrointestinal (GI) tract is the principal determinant of lethality following allogeneic bone marrow transplantation (BMT). Here, we examined the mechanisms that initiate GVHD, including the relevant antigen presenting cells. MHC-class-II was expressed on intestinal epithelial cells (IEC) within the ileum at steady state, but was absent in IEC of germ-free mice. IEC-specific deletion of MHC-II prevented the initiation of lethal GVHD in the GI tract. MHC-II expression on IEC was absent in mice deficient in the TLR adaptors MyD88 and TRIF, and required IFNγ secretion by lamina propria lymphocytes. IFNμ responses are characteristically driven by IL-12 secretion from myeloid cells. Antibiotic-mediated depletion of the microbiota inhibited IL-12/23p40 production by ileal macrophages. IL-12/23p40 neutralization prevented MHC-II upregulation on IEC and the initiation of lethal GVHD in the GI tract. Thus, MHC-II expression by IEC in the ileum initiates lethal GVHD and blockade of IL-12/23p40 may represent a readily translatable therapeutic strategy.

Graphical Abstract

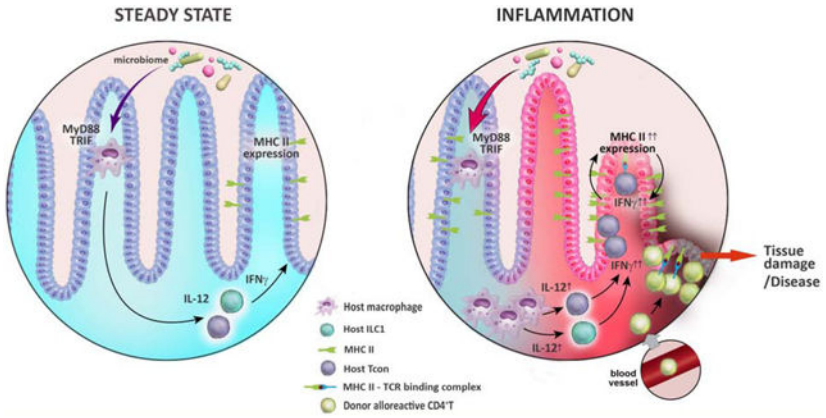

eTOC Blurb

Graft-versus-host disease in the gastrointestinal tract is the principal determinant of lethality following allogeneic bone marrow transplantation. Koyama et al. find that MHC-II dependent antigen presentation by ileal intestinal epitheial cells (IEC) is critical for the initiation of lethal GVHD in the gut, define the requirements for IEC MHC II expression and propose IL-12 neutralization as a therapeutic strategy for GVHD.

Introduction

The principal function of the immune system is to respond to pathogens in a timely and appropriate manner. This requires a balance of tightly regulated responses, especially at barrier sites, such as the skin and the gastrointestinal (GI) tract, which are continuously exposed to microbial and environmental challenges. The GI tract plays a critical role in many inflammatory conditions, including graft-versus-host disease (GVHD) following allogeneic bone marrow transplantation (BMT). Acute GVHD of the GI tract, the prima facie determinant of disease severity and lethality (Hill and Ferrara, 2000), is the manifestation of immunopathology mediated by donor T cells (Zeiser and Blazar, 2017) in response to alloantigen presented by MHC-I and MHC-II on antigen presenting cells (APC) (Koyama and Hill, 2016; Shlomchik et al., 1999). In many settings, MHC-II-dependent responses are initiated by “professional” hematopoietic-derived APC, including dendritic cells (DC), macrophages, monocytes and B cells (Kambayashi and Laufer, 2014; Unanue et al., 2016), but whether this is the case in GVHD is unclear. Non-hematopoietic cells, including mesenchymal cells and epithelial cells, can also express MHC-II when stimulated with interferon (IFN)-γ (Londei et al., 1984; McDonald and Jewell, 1987; Skoskiewicz et al., 1985); however, the physiological and pathological relevance of non-hematopoietic MHC-II expression, and the relative importance of hematopoietic versus non-hematopoietic APC populations in GI inflammation during GVHD is largely undefined.

Damage to the GI tract plays a major role in the initiation and amplification of systemic inflammation and subsequent GVHD, and fatal GVHD is almost always a consequence of GI tract involvement (Ferrara et al., 2009). The role of the microbiota in altering the severity of GVHD has been noted. Intensive antibiotic-mediated gut decontamination attenuates acute GVHD and improves survival in clinical settings, including phase III randomized studies (Beelen et al., 1999; Vossen et al., 1990). Furthermore, qualitative changes in the microbiota, particularly the loss of microbiota diversity characterized by depletion of short chain fatty acid-producing anaerobes, have been associated with impaired transplant outcome (Andermann et al., 2018; Mathewson et al., 2016). Thus, there are distinct protective and pathogenic components of the microbiota which impact on GVHD and survival following BMT.

In this study we investigated how immune responses and pathology are regulated in the GI tract in the context of allogeneic BMT, a common clinical procedure which offers a curative therapy for the majority of hematological malignancies. We focused on understanding the mechanisms controlling expression of MHC-II, as GVHD pathology is associated with $CD4^+$ T cell activity. We found that at steady state, intestinal epithelial cells (IEC) in the small intestine expressed MHC-II, but that MHC-II expression was absent in IEC from

germ-free mice. Maximal MHC-II expression on IEC required the expression of the TLR signaling adaptors MyD88 and TRIF in both hematopoietic and non-hematopoietic cells, suggesting a role for microbiota-derived TLR ligands. MHC-II expression was also regulated by cytokine signals - IL-12/23p40 from macrophages and IFNγ from lamina propria lymphocytes, including type 1 innate lymphoid cells (ILC1) and T cells. MHC-II expression on IEC increased after total body irradiation (TBI), which precedes graft transfer, concomitant with severe immunopathology in the GI tract. IEC-specific deletion of MHC-II abrogated gut pathology and lethal GVHD. Abrogation of GVHD lethality was also achieved by preventing MHC-II expression on IEC via IL-12/23p40 neutralization pre-transplant. Our findings thus define cellular and molecular pathways that initiate GVHD in the GI tract and argue for IL-12/23p40 neutralization pre-transplant as a potential therapeutic approach which can be readily tested in clinical settings.

Results

IEC in the ileum express MHC-II

The factors initiating immune pathology upon GVHD in the GI tract are unclear, including the relevant antigen presenting cell. We thus undertook an analysis of MHC-II expression in various cells and anatomical sites of the GI tract by flow cytometric analysis. MHC-II was highly and preferentially expressed in the small intestine at steady state (Figure 1A - B). A large fraction of the MHC-II expressing cells comprised Villin^{+} IEC. We then examined MHC-II expression within 4 days of BMT. Expression of MHC-II increased in the small intestine and, to a much lesser extent, in the colon (Figure 1A - B). Within the small intestine, IEC in the ileum expressed higher amounts of MHC-II than the jejunum (Figure 1C). Confocal microscopy of the ileum of mice expressing GFP under the control of the *I-A^{b}β* promoter revealed increased MHC-II transcription after conditioning with total body irradiation (TBI) (Figure 1D). The distribution of MHC-II GFP^{+} cells overlapped with that of MHC-II Ab-stained cells (Figure S1A).

The differential distribution of MHC-II in various sections of the GI tract suggested that there may be tissue site specific differences that dictate IEC responses. We compared the depth of the inner mucous layer of the colon before and early after TBI, the conditioning that proceeds transplantation, by confocal microscopy. We found that the inner mucous layer that shields IEC from bacteria remained intact in the first days following TBI (Figure 1E, Figure S1B). The mucous layer in the small intestine was less dense than the colonic inner mucous layer (Figure 1E), consistent with it being more permeable to small sized molecules (Shan et al., 2013). Concurrent staining of bacteria in the ileum of mice after TBI with a fluorescent in situ hybridization probe revealed that bacteria were present just above the villi, in direct contact with the IEC of the ileum, where an inner mucous layer was absent (Figure 1E). These findings suggest that the terminal ileum is a preferential site of mucosal-microbiota interaction, afforded at least in part by the presence of a limited mucous layer relative to that of the colon. This is consistent with data demonstrating translocation of bacteria, as determined by 16s rRNA sequencing, preferentially in the ileum (Hulsdunker et al., 2018).

MHC-II expression by IEC in the small intestine requires the microbiota

Next, we investigated the role of the microbiota in driving MHC-II expression by IEC. We could not detect MHC-II expression on the IEC ($CD45^{neg}$ epithelial cell adhesion molecule $(EpCAM)^{+}$) of germ free mice, even after TBI (Figure 2A - C, Figure S1C). In contrast, MHC-II expression by hematopoietic APC was intact in these animals, and increased after TBI (Figure 2B). In a separate approach, we treated WT mice with broad spectrum oral antibiotics (vancomycin, gentamicin, metronidazole and cefoxitin) for 2 weeks and analysed MHC-II expression in the GI tract thereafter. Depletion of the bacterial microbiota abrogated MHC-II expression on ileal IEC and prevented increased MHC-II expression on these cells after TBI, but had no impact on hematopoietic APC MHC-II expression (Figure 2D - E, Figure S1D).

In mouse models, GVHD lethality is exacerbated by dysbiosis (Varelias et al., 2017). We asked whether MHC-II expression on IEC changed under conditions of dysbiosis. WT mice were rendered dysbiotic by co-housing with *Il17ra*$^{-/-}$ mice, as previously described (Varelias et al., 2017). Flow cytometric analysis revealed increased MHC-II expression by IEC in these mice (Figure 2F - G), as well as increased donor $CD4^{+}$ T cell expansion after BMT as compared to WT mice that had not been rendered dysbiotic by prior co-housing (Figure 2H). Thus, MHC-II expression on IEC at steady state and upon inflammation requires the microbiota, and dysbiosis in a BMT setting is associated with increased IEC MHC-II expression and increased proliferation of pathogenic donor $CD4^{+}$ T cells after BMT.

MyD88 and TRIF signalling are necessary for MHC-II expression by IEC

We then asked whether MHC-II on IEC could promote the activation and proliferation of naïve $CD4^{+}$ T cells using an HY male antigen-specific TCR transgenic system (Marilyn T cells that recognize male peptide complexed within I-A^{b}) (Lantz et al., 2000). We co-cultured sort purified IEC collected from female or male mice 20 hours after TBI with CFSE-labelled Marilyn T cells and examined Marilyn T cell activation and proliferation 7 days later by measuring CD69 expression and CFSE dilution respectively. We found that male ileal MHC-II^{+} IEC could stimulate Marilyn T cells (Figure 3A, Figure S2A - B). Ileal MHC-II^{+} IEC did not express costimulatory molecules at steady state, but exhibited increased expression of CD80 after TBI (Figure S2C - D), and inhibition of CD80 in the co-cultures with an anti-CD80 monoclonal antibody attenuated the stimulatory capacity of IEC after TBI (Figure S2E). Thus, IEC MHC-II expression can drive the proliferation of naïve $CD4^{+}$ T cells.

We then focused on the molecular mechanisms controlling MHC-II expression in IEC at steady state, before and after BMT. We performed RNAseq analysis using sort-purified IEC ($CD45^{neg}$ Villin-YFP^{+}) from the small intestine of naïve mice, mice post-TBI, and mice post-BMT (after TBI and with grafts including T cells) (Figure 3B). Principal component analysis (PCA) of gene expression profiles separated naïve mice from the other two groups, indicating that the transcriptional landscape of IEC is most influenced by TBI (Figure 3C). Single-sample gene-set enrichment analyses (ssGSEA) indicated that expression of genes associated with antigen presentation and processing pathways was augmented both in mice

receiving TBI alone and those receiving T cell replete grafts that developed GVHD (Figure 3D, Figure S2F, Figure S3). These pathways appeared in three distinctive clusters. Cluster 1 included genes involved in cell cycle and transcription. Multiple pathways related to antigen processing were tightly linked in cluster 2. Cluster 3 involved MHC-II antigen presentation pathways, together with toll-like receptor (TLR) driven signalling cascades, including multiple pathways downstream of TLR3 and TLR4 (Figure 3D and Figure S2F, Figure S3).

Given the juxtaposition of IEC and the gut microbiota, and the importance of the latter to GVHD (Hayase et al., 2017; Jenq et al., 2012; Shono et al., 2016), we investigated the relationship between TLR signalling and MHC-II antigen presentation in the GI tract. We compared the ileum and colon from naïve B6 mice (B6.WT) and mice deficient for the TLR signalling adaptors MyD88 and TRIF (B6.*Myd88*$^{-/-}$ *Trif*$^{-/-}$). MHC-II expression in hematopoietic populations (CD45^{+} EpCAM^{neg}) of B6.WT and B6.*Myd88*$^{-/-}$ *Trif*$^{-/-}$ mice was comparable. However, IEC (CD45^{neg} EpCAM^{+}) from B6.*Myd88*$^{-/-}$ *Trif*$^{-/-}$ mice lacked MHC-II expression both at steady state and after TBI (Figure 3E - F and Figure S4A). In order to determine the relevance of this pathway to donor T cell expansion, we transplanted luciferase-expressing Marilyn T cells into male B6.WT or B6.*Myd88*$^{-/-}$ *Trif*$^{-/-}$ recipients and measured their proliferation. T cell expansion was reduced in the small intestine but not in the colon or spleen of B6.*Myd88*$^{-/-}$ *Trif*$^{-/-}$ recipients (Figure 3G), consistent with the expression pattern of MHC-II on IEC. Furthermore, higher frequencies of Marilyn T cells were detected in the draining mesenteric lymph nodes (mLN) of WT recipients as compared to *Myd88*$^{-/-}$ *Trif*$^{-/-}$ recipients, and these cells expressed the transcription factor T-bet, a hallmark of Th1 differentiation (Figure 3H). To determine whether the requirement for TLR signalling in IEC MHC-II expression lay within the hematopoietic or the non-hematopoietic compartment, we used BM chimeras in which hematopoietic cells, non-hematopoietic cells or combinations thereof were deficient in Myd88 and TRIF. Expression of MyD88 and TRIF was required in both hematopoietic and non-hematopoietic compartments for the full induction of MHC-II expression on IEC (Figure S4B - C).

IFNγ is secreted by recipient ILC1 and conventional T cells in the small intestine

We next examined the role of IFNγ in IEC MHC-II expression as this cytokine is known to potently induce MHC-II expression in epithelial cells (Skoskiewicz et al., 1985). IEC from B6 WT mice expressed the IFNγ receptor (IFNγR) at steady state as measured by flow cytometry (Figure 4A), and B6.*Ifngr*$^{-/-}$ mice did not express MHC-II on IEC, either at steady-state or after TBI (Figure 4B - C and Figure S4A). To delineate the potential sources of IFNγ driving the expression of MHC-II, we analyzed MHC-II expression in the intestine of *Rag*$^{-/-}$ *Il2rg*$^{-/-}$ mice, which lack innate and adaptive lymphocyte populations, and *Rag*$^{-/-}$ mice, which lack conventional TCR-rearranged T cells, pre and post-TBI. MHC-II expression in the ileum was lost in *Rag*$^{-/-}$ *Il2rg*$^{-/-}$ mice and decreased in *Rag*$^{-/-}$ mice (Figure 4D and Figure 4E). Flow cytometric analysis of lamina propria lymphocytes from naïve *Ifng*-YFP reporter mice demonstrated that, amongst innate cell populations, IFNγ expression was predominantly in CD200r^{+} ILC1 (Weizman et al., 2017) (Figure 4F and Figure S5B - C). In naïve mice, IFNγ expression was also observed in adaptive lymphocytes, primarily CD4^{+} T cells (Figure 4F). MHC-II expression in the ileum of *Rag*$^{-/-}$ mice did not increase after TBI (Figure 4E, Figure S5A). Indeed, the TBI-induced IFNγ was

predominantly observed in conventional T cells ($CD4^+$ Tcon, $CD8^+$ Tcon) and to a smaller extent NKT cells, rather than innate lymphocyte populations, and was primarily seen in conventional T cells in the GI tract, but not in T cells in the draining mLN (Figure 4G, Figure S5D). In order to determine whether the induction of MHC-II expression by IEC was a direct effect of IFNγ, we cultured intestinal organoids from the small intestine of B6.*I-A*^{b} β-GFP or B6.WT mice with or without IFNγ. $EpCAM^+$ epithelial cells in organoids did not express MHC-II under standard culture conditions, but did so rapidly in the presence of IFNγ (Figure 4H and Figure S5E). IFNγ also induced MHC-II expression (HLA-DR/DQ/DP) in human small intestine organoid cultures (Figure 4I). Taken together, these results suggest that MHC-II expression on IEC in the ileum can induce localized T cell activation and IFNγ secretion, and in the context of GVHD, TBI induces a local cytokine feed-forward cascade that amplifies MHC-II expression on IEC.

IEC are sufficient to induce MHC-II-dependent GVHD

We next investigated whether MHC-II antigen presentation by IEC could initiate acute GVHD. We previously demonstrated that host non-hematopoietic APC, including cells of mesenchymal origin, can also express MHC-II (Koyama et al., 2012). We therefore used three murine lines expressing Cre-recombinase (Cre) driven off *Villin*, *Nestin* and *Tie2* promoters, which are lineage markers for IEC, mesenchymal and endothelial cells respectively, to define the relevance of MHC-II expressed by these non-hematopoietic cell populations in the GI tract in driving GVHD. Lineage-restricted expression in the intestine was determined by Cre-driven YFP expression. Villin-expressing cells were $EpCAM^+CD45^{neg}$ epithelial cells and aligned on the surface of villi. Nestin-expressing cells were $CD45^{neg}Vimentin^+$α-smooth muscle actin $(αSMA)^+$, consistent with mesenchymal cells. $CD45^{neg}$ Tie2-expressing cells were $CD31^+Ter119^{neg}$ endothelial cells (Figure 5A and Figure S6A). $I\text{-}A^b$ is the MHC-II molecule expressed in B6 mice, and its expression can be deleted in Cre-expressing (Cre^{pos}) cell lineages using a floxed *I-A*^{b} gene (*I-A*$^{b\text{-}fl/fl}$) (Hashimoto et al., 2002). Next, we compared GVHD lethality between transplanted mice in which lineage restricted non-hematopoietic cells can (Cre^{neg}) or cannot (Cre^{pos}) present MHC-II-loaded alloantigen. B6 male *Nestin*, *Villin* or *Tie2* Cre^{pos} *I-A*$^{b\text{-}fl/fl}$ mice and relevant Cre^{neg} *I-A*$^{b\text{-}fl/fl}$ mice were reconstituted with female *I-A*^{b} deficient bone marrow (B6.*I-A*$^{b-/-}$ BM), thus generating BM chimeras lacking the capacity for antigen presentation by hematopoietic APC (Figure S6B - D). Three months later, these BM chimeras were used as BMT recipients and transplanted with female B6.*I-A*$^{b-/-}$ BM (to reconstitute hematopoiesis whilst preventing Ag presentation by donor APC) and Marilyn T cells. GVHD mortality invoked by Marilyn T cells in response to alloantigen presented in recipient MHC-II was initiated by Villin-expressing cells, and less so Nestin-expressing cells (Figure 5B). A significant reduction in luciferase-expressing Marilyn T cell expansion in the gut was also noted when recipient Villin-expressing cells alone could not present antigen (Figure 5C). Thus, MHC-II expression on IEC can initiate lethal GVHD immune responses.

MHC-II-expressing IEC are necessary for the induction of $CD4^+$ T cell-dependent GVHD within the GI tract

We examined the role of Villin-expressing cells in lethal acute GVHD using a second experimental system where recipients express Tamoxifen-dependent Cre-recombinase under

the control of the *Villin* promoter (*Villin*Cre-ER^{T2}) (Adolph et al., 2013; el Marjou et al., 2004). This allowed us to interrogate the role of IEC as APC in a physiologically relevant manner whereby donor and host hematopoietic APC are intact, but mice have (Cre-ER$^{T2\text{-}neg}$*I-A*$^{b\text{-}fl/fl}$), or lack (Cre-ER$^{T2\text{-}pos}$*I-A*$^{b\text{-}fl/fl}$) MHC-II specifically on IEC after Tamoxifen administration (Figure S6E - F). Despite the presence of all other types of APC, the lack of MHC-II^{+} IEC resulted in profound protection from acute GVHD lethality (Figure 6A). Consistent with this, these mice exhibited reduced levels of serum TNF (Figure 6B), decreased Marilyn T cell expansion in the gut and mLN, but not other peripheral sites (Figure 6C - D, Figure S7A). In addition, a lower frequency of Marilyn T cells recovered from the mLN of these mice expressed T-bet, (Figure 6E, Figure S7B), and GVHD pathology in the GI tract was ameliorated (Figure 6F - G). We corroborated these findings in an allogeneic system where GVHD was mediated by polyclonal T cells. Wild type (WT) polyclonal CD4^{+} T cells from BALB/c mice (H-2^{d}) were transplanted into MHC-mismatched female *Villin*Cre-ER$^{T2\text{-}neg}$*I-A*$^{b\text{-}fl/fl}$ or Cre-ER$^{T2\text{-}pos}$*I-A*$^{b\text{-}fl/fl}$ recipients (H-2^{b}). *Villin*Cre-ER$^{T2\text{-}pos}$*I-A*$^{b\text{-}fl/fl}$ recipients did not develop gut GVHD in this setting (Figure 6H - J), although they did develop severe cutaneous GVHD that eventually required the mice to be euthanized (Figure 6K). Thus, in this scenario, polyclonal donor CD4^{+} T cells could be primed and redirected by alternate APC to other GVHD target organs (e.g. skin).

IL-12 neutralization prevents MHC-II expression by IEC pre-transplant and averts CD4^{+} T cell-dependent GVHD lethality.

Next, we examined the effects of pre-transplant microbiota depletion on GVHD in the GI tract and the role of donor T cell-derived IFNγ on the expression of MHC-II by IEC after BMT. We transplanted male recipients, who had or had not received antibiotic-mediated microbiota decontamination, with Marilyn T cells. Three days after transplant, MHC-II expression on IEC remained low in microbiota depleted recipients and was similar to non-GVHD controls (Figure 7A). In conjunction with this, T-bet expression also remained low in recipient ILC1 (Figure 7B). Nevertheless, systemic IFNγ was produced in microbiota-depleted recipients receiving donor alloreactive T cells by day 3 after BMT, albeit at a lower level than recipients with an intact microbiota (Figure 7C). Consistent with this, MHC-II expression increased in these recipients by day 7 after transplant, although this did not reach the levels seen in animals where the microbiota was intact (Figure 7D). Marilyn T cell infiltration in the gut of microbiota-depleted recipients was markedly attenuated, and acute GVHD histopathology was prevented (Figure 7D). We next explored the role of IL-12 in the IFNγ dependent induction of MHC-II expression by IEC, since IFNγ responses are characteristically driven by IL-12 secretion from myeloid lineages (Biron and Tarrio, 2015). Flow cytometric analysis of B6.*IL-12/23p40*-YFP mice demonstrated that IL-12/23p40 was preferentially expressed by macrophages and, to a lesser extent, DC in ileum lamina propria preparations (Figure 7E), and that IL-12 expression increased after TBI (Figure 7F). Antibiotic treatment reduced the number of IL-12/23p40-YFP^{+} cells in the ileum of mice pre-transplant (i.e. post TBI, pre-cell infusion) (Figure 7G - H). Mice treated with anti-IL-12/23p40 prior to TBI did not exhibit increased MHC-II expression by IEC pre-transplant (Figure 7I and Figure S7C), and this treatment decreased acute GVHD lethality (Figure 7J). Finally, the expression of MHC-II by IEC in the ileum pre-transplant was abrogated in

Il12p35$^{-/-}$ recipients, pointing to a critical role for IL-12 in IEC MHC-II expression (Figure S7D).

Discussion

Gut pathology is a key initiator of GVHD after allogeneic BMT. Characterization of the cellular and molecular mechanisms that initiate gut disease is key to identifying pathways that can be targeted therapeutically. Here we established a pivotal role for IEC in MHC-II-dependent antigen presentation and thereby, in the initiation of GVHD in the GI tract. We also showed that the microbiota controlled MHC-II expression by IEC, both at steady-state and during inflammation induced by conditioning. This required an IL-12/IFNγ cytokine axis that could be targeted therapeutically to block CD4$^+$ T cell-dependent GVHD.

The interactions between the microbiota and host immunity are well-defined and involve various DAMP/PAMP signalling motifs, including TLRs, Nod-like receptors and short-chain fatty acids (Chang et al., 2014; Vatanen et al., 2016). However, the ability of the microbiota to shape antigen presentation by gut epithelial cells has not been defined. Although MHC gene expression in the GI tract is linked to the microbiota (El Aidy et al., 2012), the cell subsets involved and subsequent responses therein, have not been delineated. MHC-II expression on IEC, most highly in intestinal stem cells, controls epithelial-cell remodelling following infection (Biton et al., 2018); however, whether this MHC-II expression has a pathogenic role in the induction of disease is unknown. Here, we showed that 1) under homeostatic conditions, IL-12 secretion from macrophages induced IFNγ secretion by lamina propria lymphocytes in a microbiota and MyD88/TRIF-dependent manner, resulting in MHC-II expression by IEC in the ileum and 2) that MHC-II expressing IECs functioned as APCs to prime donor CD4$^+$ T cells in vivo and induced lethal acute GVHD. Furthermore, conditioning with TBI invoked additional IL-12 secretion by macrophages in a microbiota-dependent manner and rapid IFNγ secretion by conventional T cells in the GI tract, which resulted in rapid and marked enhancement of MHC-II expression, together with CD80 expression by IEC. Critically, deletion of MHC-II in Villin-expressing enterocytes prevented disease by restraining donor CD4$^+$ T cell priming, differentiation and GVHD in the GI tract. Reduced T-bet expression in T cells in the mLN was noted, and we speculate that these cells migrate from the small intestine after priming, as previously described (Beura et al., 2018). Thus, we describe interactions between the microbiome and immune cells in the GI tract pre-transplant and show that when this balance is perturbed by inflammatory signals during conditioning, overt immunopathology ensues.

Our results have identified an axis of antigen presentation that drives disease in the GI tract after BMT, and have defined pathways for therapeutic intervention that can be immediately tested. While it is clear that hematopoietic cells include the principal APC that drive MHC class I-dependent acute GVHD (Shlomchik et al., 1999; Toubai et al., 2012), this does not hold true for MHC-II-dependent acute GVHD (Koyama et al., 2012). While acute GVHD can be mediated by MHC-II expressing hematopoietic cells (Teshima et al., 2002), there has been no direct comparison with MHC-II expressing non-hematopoietic cells, which appear dominant (Koyama et al., 2012). Here we demonstrated that the initiation phase of MHC-II-dependent acute GVHD required a cognate CD4$^+$ T cell-MHC-II interaction at the intestinal

epithelial surface. We also showed that MyD88/TRIF pathways in both the hematopoietic and non-hematopoietic compartment were involved, consistent with the fact that inhibition of these pathways in the hematopoietic compartment only is insufficient to block MHC-II antigen presentation in the GI tract, and subsequent GVHD (Li et al., 2011). While non-hematopoietic cells may also respond to microbiota-derived signals to induce MHC-II expression on IEC and should be the subject of further study, in our studies the inhibition of microbiota-driven IL-12 pre-transplant was sufficient to attenuate MHC-II expression by IEC and prevent acute GVHD lethality. Thus, we have identified IEC as the non-hematopoietic APC involved in antigen presentation thereby explaining the inability of approaches that delete hematopoietic professional recipient APC to prevent acute GVHD in preclinical systems (Hashimoto et al., 2011; Koyama et al., 2012; Li et al., 2012; MacDonald et al., 2010; Rowe et al., 2006). It is important to note that many professional APC subsets (e.g. DC) do potently present alloantigen, but the net effect of this function is activation-induced cell death and/or phagocytosis (e.g. by macrophages) of donor $CD4^+$ T cells, which paradoxically attenuates GVHD (Hashimoto et al., 2011; Koyama et al., 2012; Markey et al., 2018). Thus, approaches to delete recipient DC, macrophages or even B cells are generally deleterious, and instead amplify GVHD. In contrast, IEC presented endogenous alloantigen in a truly pathogenic fashion (since deletion attenuated GVHD) and this process was under strict control by soluble mediators secreted by hematopoietic APC (i.e. IL-12) and lymphocytes (i.e. IFNγ) induced in response to the microbiota pre-transplant. Although the mechanisms whereby the microbiome plays an important role in disease penetrance and phenotypes, including GVHD, are not understood (Jenq et al., 2012; Shono et al., 2016), it is clear that the transfer of dysbiotic GI tract microbiota can alter GVHD phenotypes (Varelias et al., 2017). The current data suggest that the control of antigen presentation within IEC is an important component of this interactive network that should now be explored in other inflammatory diseases of the GI tract, particularly Crohn's disease, where the terminal ileum is selectively involved. Finally, the role of DAMPs in this process is unclear and deserves further study.

The secretion of IFNγ by conventional recipient T cells within 24 hours of TBI, in the absence of transplantation, was unexpected. Since this did not occur in secondary lymphoid organs despite significant IL-12 secretion at those sites, it seems that localized, likely tissue resident memory T cells respond to local TCR-dependent signals in the context of IL-12. It is likely that this reflects a response to local pathogen-derived peptide-MHC complexes that are absent in tissue-draining lymph nodes and drives a tissue specific feed forward cascade in the GI tract. Systemic neutralisation of IL-12, commencing before TBI, prevented the increase of IFNγ-dependent expression of MHC-II by IEC that initiated acute GVHD. This finding is consistent with the fact that exogenous IL-12 administration after TBI exacerbates gut GVHD (Hixon et al., 2002). A number of lines of evidence suggest that IFNγ acts directly on IEC to invoke antigen presentation. Firstly, the addition of exogenous IFNγ to organoids that do not contain hematopoietic cells induced MHC-II expression. Secondly, the ability of IFNγ to induce intestinal GVHD requires expression of the IFNγR on parenchymal cells only (Burman et al., 2007). IFNγ from donor $CD4^+$ T cells may damage MHC-II expressing IEC indirectly, without cognate MHC-TCR interaction, as previously described (Teshima et al., 2002) and this deserves further study. The inhibition of IFNγ

itself after BMT results in severe acute lung injury (Burman et al., 2007; Varelias et al., 2015), and thus this approach is not feasible in the clinic. IFNγ can be generated by alloreactive donor T cells in response to APCs that are not IECs, and this can in turn augment MHC-II expression by IEC. The fact that IEC in antibiotic-treated mice expressed MHC-II post-transplant (i.e. beyond day 3), yet there was no significant T cell expansion or gut GVHD by histopathology relative to non-GVHD controls, is consistent with the notion that it is the early expression of MHC-II (prior to day 3) on IEC that is critical in initiating gut GVHD.

Nevertheless, this pathway has the potential to invoke a feed-forward loop of antigen presentation by IEC after transplant that is generated by the alloreactive T cell itself. That said, this phenomena is likely to be less relevant in clinical transplantation where T cell-dependent effector cytokine responses, including IFNγ, are prevented by standard immune suppression with calcineurin inhibitors and methotrexate early after BMT (Kennedy et al., 2014).

Our results demonstrated that the microbiota controls MHC-II on IEC pre-transplant (including after TBI but pre-cell infusion) and that this pathway can contribute to the initiation of GVHD. However, this does not exclude additional effects of the microbiota after transplant that may be independent of MHC-II expression by IEC. This includes the activation of other APC and T cells that will contribute to the kinetics of GVHD, and these pathways should continue to be investigated. Given the successful therapeutic application of IL-12 inhibition to treat Crohn's disease (Feagan et al., 2016), and promising early results in BMT targeting T cell differentiation after transplant (Pidala et al., 2018), IL-12 inhibition starting before conditioning would appear an attractive adjunct approach to prevent GVHD. Intriguingly, our data also suggest that strategies to prevent GVHD based on host T cell depletion would be most efficacious when completed prior to the initiation of conditioning. It is also important to note that pretransplant inhibition with clinical IL-12 blocking antibodies that have a half-life of many weeks (Pidala et al., 2018) may also minimize the aforementioned feed-forward loop of antigen presentation by IEC in response to donor T cell-derived IFNγ after BMT.

The crucial role for antigen-presentation by IEC in the ileum as a distinct anatomical site is intriguing, particularly given that the colon is the site where most microbiota-derived PAMP signals reside. Despite this, colon epithelial cells did not express high levels of MHC-II even after BMT, likely reflective of effective barrier function, including the extensive mucous layer present at this site, as opposed to the ileum. Indeed, recent studies confirm that the ileum is the anatomically weakest barrier site in the GI tract (Hulsdunker et al., 2018).

Although MHC-II expression by non-hematopoietic cells such as fibroblasts, endothelial cells and epithelial cells has been described (Londei et al., 1984; Saada et al., 2006; Stevanovic et al., 2013), its functional role in antigen presentation has remained ambiguous. Indeed, it has been considered to promote tolerance rather than inflammation (Kambayashi and Laufer, 2014; Thelemann et al., 2014). In relation to gut epithelia, HLA class II is expressed in the colon during GVHD or in infectious colitis after renal transplant (Stevanovic et al., 2013). Furthermore, colonic epithelial cells express HLA-DR in non-

transplant patients with IBD and infectious colitis, whereas this is not the case in healthy donors (McDonald and Jewell, 1987). In addition, since the role of MHC-II is classically defined by exogenous antigen presentation following phagocytosis or endocytosis, the relative importance for endogenous antigen presentation, including alloantigen presentation, by MHC-II is less clear (Paludan et al., 2005; Roche and Furuta, 2015). Our results demonstrated that IEC presented alloantigen to $CD4^+$ T cells and could initiate GVHD, a finding with major implications for the pathogenesis of other inflammatory conditions involving the GI tract. Furthermore, our data highlighted a number of critical pathways that can be modulated prior to transplant to prevent the initiation of acute GVHD in the GI tract, focusing on the microbiota, PAMP signalling and the downstream cytokines IL-12 and IFNγ.

STAR Methods

Mice.

C57BL/6J (B6.WT, H-2^b, $CD45.2^+$), BALB/c (H-2^d, $CD45.2^+$) and B6D2F1 (H-$2^{b/d}$, $CD45.2^+$) were purchased from the Animal Resources Centre, Perth, AUS. B6.*Rag1*$^{-/-}$ and B6.*Rag2*$^{-/-}$*Il2rg*$^{-/-}$ mice were obtained from the QIMR Berghofer animal facility. Transgenic and knockout mice on a B6 background originated as follows: *H2-A*^{b}*1*$^{-/-}$, referred to as B6.*I-A*$^{b-/-}$, Australian National University, Canberra, AU; *Villin*Cre-ER^{T2}, Dr R Blumberg, Harvard Medical School, Boston, MA, USA (Adolph et al., 2013; el Marjou et al., 2004); *Rosa26*-YFP, Dr B. Stockinger, MRC National Institute for Medical Research, Mill Hill, London, UK (Hirota et al., 2011); *β-actin*-luciferase C57BL6 and BALB/c, Dr Robert Negrin, Stanford, CA, USA (Beilhack et al., 2005); Marilyn Tg (*Rag2*$^{-/-}$ background), Dr P Matzinger, NIH, Bethesda, MD, USA (Lantz et al., 2000); B6. *I-A*^{b}*β*-GFP, Dr Barbara Fazekas de St Groth, Garvan Institute, Sydney, AU; 2011); B6.*MyD88*$^{-/-}$*Trif*$^{-/-}$, Dr S Akira, Osaka University, Osaka, Japan (Yamamoto et al., 2003); B6.*Il17ra*$^{-/-}$ as previously described (Varelias et al., 2017); *I-A*$^{b\text{-fl/fl}}$ (Stock 013181, B6.129X1-*H2-Ab1*^{tm1Koni}*/J*) (Hashimoto et al., 2002), *Villin*-Cre (Stock 004586, B6.SJL-*Tg(Vil-cre)997Gum*/J), *Nestin*-Cre (Stock 003771, B6.Cg-*Tg(Nes-cre)1Kln*/J), *Tie2*-Cre (Stock 008863, B6.Cg-*Tg(Tek-cre)1Ywa*/J), B6.*Il12/23p40*-YFP (Stock 006412, B6.129-*Il12b*^{tm1Lky}/J), B6.*Ifnγ*-YFP (Stock 017581, B6.129S4-*Ifng*$^{tm3.1Lky}$/J) , B6.*Ifnγr*$^{-/-}$ (Stock 003288, B6.129S7-*Ifngr1*^{tm1Agt}/J) and *IL-12p35*$^{-/-}$ (Stock 002692, B6.129S1-*Il12a*^{tm1Jm}/J), the Jackson Laboratory, Bar Harbor, MA, USA. *Rag2*$^{-/-}$ background Marilyn mice were backcrossed onto a B6 *β-actin*-luciferase background (Marilyn^{luc+}, $CD90.1^+$ $CD45.2^+$). Each of the Cre strains and *I-A*$^{b\text{-fl/fl}}$ or *Rosa26*-YFP strains were intercrossed to generate *Villin*Cre *I-A*$^{b\text{-fl/fl}}$, *Villin*Cre-ER^{T2} *I-A*$^{b\text{-fl/fl}}$, *Nestin*Cre *I-A*$^{b\text{-fl/fl}}$, *Tie2*Cre *I-A*$^{b\text{-fl/fl}}$, *Villin*Cre *Rosa26*-YFP, *Nestin*Cre *Rosa26*-YFP and *Tie2*Cre *Rosa26*-YFP mice. Mice were bred at the QIMR Berghofer animal facility. B6.WT mice were housed under germ free conditions at the University of Queensland Biological Resources Facility (UQBRF). For cohousing experiments, mice were housed as described previously (Varelias et al., 2017). Mice were housed in sterilized microisolator cages and received acidified autoclaved water (pH 2.5) after transplantation. Experiments were performed with sex and age-matched animals using littermates where possible.

Stem Cell Transplantation.

B6 or B6D2F1 mice were transplanted as described previously (Koyama et al., 2012) with 1000 cGy or 1100 cGy total body irradiation (TBI, 137Cs source at 84 cGy/min) on day −1, respectively. On day 0, B6 mice were transplanted with 5×10^6 bone marrow (BM) cells and ($0.025 – 0.5 \times 10^6$) luciferase-expressing Marilyn cells. BM cells were depleted of T cells by antibody and complement as previously described (T cell depletion = TCD). Marilyn $CD4^+$ T cells (*RagT*$^{-/-}$ background) were purified to greater than 98% by sorting of $V\beta6^+$ $CD8^{neg}$ cells using a MoFlo (Beckman Coulter) or 70% by CD4 MACS system (Miltenyi). To generate MHC-II deficient BM chimeric mice, the relevant lethally irradiated Cre-^{neg}*I-A*$^{b\text{-}fl/fl}$ and Cre-^{pos}*I-A*$^{b\text{-}fl/fl}$ mice were injected with 10×10^6 female B6.*I-A*$^{b-/-}$ BM and treated with anti-CD4 (GK1.5) and CD8 (53-5.8) mAbs. The Abs were administrated i.p. from day −2 (GK1.5; 500μg/ animal, 53-5.8; 150μg/ animal) followed by weekly injection (GK1.5; 250μg/animal, 53-5.8; 150μg/animal) until week 6 to prevent any persistence of recipient T cells in a class II negative environment. Five weeks after Ab discontinuation, the BM chimeric mice were used in secondary transplants. For BMT utilizing WT polyclonal $CD4^+$ T cells, lethally irradiated female mice were transplanted with 5×10^6 BM and 5×10^6 $CD4^+$ T cells (MACS purified) from Treg-depleted BALB/c donor mice (PC61; 500μg/ animal, day −3 and −1, i.p.). Tamoxifen (1mg/day) was administered for 5 days, 2 weeks before transplant where indicated. IL-12p40 (C17.8) or control rat IgG2a (MAC4) was administered intraperitoneally at 500μg per dose on days −2 and −1 prior to TBI, and on the day of transplant (d0) prior to the infusion of graft (BM and T cells). In BMT using B6D2F1 recipients, lethally irradiated female B6D2F1 mice were transplanted with 5×10^6 BM and 2×10^6 T cells from B6.WT mice using magnetic bead depletion as previously described (MacDonald et al., 2010). Animal procedures were undertaken using protocols approved by the institutional (QIMR Berghofer) animal ethics committee. The severity of systemic GVHD was assessed by scoring as previously described (maximum index = 10) (Cooke et al., 1996). For survival experiments, transplanted mice were monitored daily and those with GVHD clinical scores ≥ 6 were sacrificed and the date of death registered as the next day, in accordance with institutional guidelines.

Cell isolation from small intestine and colon.

Longitudinally sectioned pieces of the small intestine or the colon were processed using a gentleMACS Dissociator and mouse lamina propria dissociation kit (both Miltenyi Biotec), according to the manufacturer's protocol. Dithiothreitol was excluded from the entire process. We sectioned the small intestine into the proximal third (duodenum), the middle third (jejunum) and the distal third (ileum).

Gut decontamination.

For microflora depletion, an antibiotic cocktail of vancomycin, metronidazole, cefoxitin and gentamicin (final concentrations 1 mg/ml each) was added to the drinking water for 14 days before TBI (Hulsdunker et al., 2018). Control mice received acidified water (pH 2.5) without antibiotics.

Mouse and human organoid isolation and growth protocol.

The small intestine was isolated from naïve WT.B6 and B6.*I-A^{b}β*-GFP reporter mice. After rinsing with HBSS without Ca and Mg, the small intestine was cut into 1mm pieces and incubated for 15 minutes in dissociation buffer consisting of PBS and 0.02M EDTA. After physical separation, crypts were counted on a hemocytometer with trypan blue and 200 viable crypts per well were suspended in 50% type 2, PathClear Cultrex® reduced growth factor basement membrane extract. After the basement membrane was set at 38°C, 500μL of 50% conditioned media derived from the L-WRN cell line, and including ALK5 kinase inhibitor and p160ROCK inhibitor, was added to each well and grown at 38°C (Miyoshi and Stappenbeck, 2013). Growing enteroids were enumerated at day 5 with media changed every 2-3 days. 10ng/mL of recombinant murine IFNγ or diluent was added to growth media for 24 hours prior to isolation and staining for confocal microscopy. Live organoids were stained with DAPI (1/1000) and BioLegend AF647 anti-mouse CD326 (EpCAM). Human intestinal organoids from the duodenal tissue of 3 healthy donors were generated by the same method as above and stained with PE-conjugated anti-HLA DR+DP+DQ (Abcam), CD45 AF647 and CD326 AF488 (BioLegend) for flow cytometric analysis. The procedures were undertaken using protocols approved by the University of Queensland ethics committee.

Flow cytometry.

For surface staining, cell suspensions were incubated with anti-CD16/CD32 (2.4G2) followed by staining with antibodies against CD45.2, CD31, Ter119, MHC class II (I-A/I-E), CD69, CD326 (EpCAM), CD19, CD3, TCRβ TCRγδ, CD4, CD8, NKp46, Ly6G, CD11c, CD64, CD11b, CD40, CD80, CD86, Rat IgG2a isotype control, Armenian Hamster IgG isotype control, Rat IgG2b isotype control and T-bet (all BioLegend); CD90.1, YAe and CD200r (eBioscience); Vβ6, CD19, DX5 (CD49b), NK1.1, Ly6C and IFNγR1 (CD119) (BD Biosciences). 7AAD (Sigma) was added before cell acquisition. For intracytoplasmic staining (villin and vimentin (Abcam, Cambridge, UK) and αSMA (eBioscience)), single-cell suspensions were incubated with fixable live/dead cell dye (ThermoFisher), FcγR blocked with 2.4G2 and stained for surface markers. Cells were then fixed and permeabilized using the BD Fix/Perm kit (BD) according to the manufacturer's protocol and stained with Abs against villin, vimentin or αSMA for 30 min at room temperature, washed and acquired. T-bet expression was determined using the Foxp3 staining buffer set (eBioscience) according to the manufacturer's protocol. Samples were acquired with a BD LSRFortessa (BD) and analysis was performed with FlowJo v9 (Tree Star) software. Representative flow cytometry plots display concatenated replicates from one experiment.

Histologic analysis.

H&E stained sections of formalin-fixed tissue were coded and examined in a blinded fashion by A.D.C. using a semi-quantitative scoring system, as previously described (Koyama et al., 2012). Images of GVHD target tissues were acquired using an Olympus BX51 microscope (Olympus), an Evolution MP 5.0 Camera, and Qcapture software (Qimaging).

Immunofluorescence microscopy.

Tissues were fixed with 4% paraformaldehyde, then placed in 30% sucrose prior to being frozen in Tissue-Tek OCT compound (Sakura Finetek). Sections (7μm thickness) were treated with Background Sniper (Biocare Medical) and 2% BSA for 30 min and then stained with IA/IE PE (isotype Rat IgG2b PE) and CD45-Alexa flour 647 (isotype Rat IgG2b AF647) (all mAbs; BioLegend) for 120 min at room temperature in the dark. After washing, sections were counterstained with DAPI for 5 min and cover-slipped with Vector Vectashield Hard Set mounting media. Samples for quantitation of mucus thickness were prepared as described (Johansson et al., 2008). In brief, samples were fixed in Methacarn solution (60% methanol, 30% chloroform, 10% glacial acetic acid, Sigma) for *6h,* washed in methanol followed by ethanol and xylol, and embedded in paraffin. Slides were deparaffinized and washed in ethanol. *In situ* hybridization was performed at 46° C for 16*h* in a hybridization buffer (0.9 M NaCl, 20 mM Tris/HCl, 0.01 % sodium dodecyl sulfate (SDS), 20 % formamide) containing a eubacterial probe Eub338 (Cy3-GCTGCCTCCCGTAGGAGT) and non-Eub (6-FAM-ACTCCTACGGGAGGCAGC) (each 10ng/μl). Slides were washed in washing buffer (0.225 M NaCl, 20 mM Tris/HCl, 0.01 % SDS, 5 mM EDTA) for 15 min, then in PBS and blocked in PBS containing 4 % FCS. Polyclonal Muc2 antibody was applied for 4-16*h* at 4°C followed by incubation with secondary anti-rabbit Alexa Fluor 647 antibody for 1-2*h* at 4°C and DAPI for counterstaining. Images were taken with x40 oil-immersion lens or x10 non-oil lens using a Zeiss 780-NLO Point Scanning Confocal Microscope with Zen software (Zen software). For quantification of MHC-II expression by IEC, mean fluorescence intensity (MFI) was measured with ImageJ 1.51w software, whereby each data point represents the average from the epithelial layer of 9-15 villi from 3-5 high-power fields per animal, standardized to expression within naïve WT (Figure 3,4,7) or MHC-II-GFP (Figure 1) animals (fold-change).

Mixed lymphocyte reaction (MLR).

Carboxy fluorescein diacetate succinimidyl ester (CFSE) labelling was performed as described (Koyama et al., 2015). In round-bottom 96-well plates, sort-purified CFSE-labeled Marilyn^{luc+} cells (CD90.1^{+}) were stimulated with sort-purified intestinal epithelial cells (IEC) (CD326^{+}CD45.2^{neg}) from the small intestine of female or male B6.WT mice which had undergone TBI 20*h* before, in the presence of rhIL-2 (100 U/ml) (Zhang et al., 2017). Seven days later, Marilyn^{luc+} T cells (CD90.1^{+}CD4^{+}CD45.2^{+}) were assessed for CFSE dilution and expression of CD69 by flow cytometry. For CD80 blocking, purified CD80 mAb (clone 16-10A1, BioLegend) or its isotype control (Armenian Hamster IgG, BioLegend) was added to cultures at 1μg / ml.

Cytokine analysis.

Serum TNF levels were determined using the BD Cytometric Bead Array system (BD Biosciences Pharmingen) according to the manufacturer's protocol.

Bioluminescence imaging (BLI).

T cell expansion was determined by analysis of luciferase signal intensity (Xenogen IVIS 100; Caliper Life Sciences). Light emission is presented as photons per second per square

centimeter per steer radiant (ph/s/cm2/sr). Total flux of mouse or organ is presented as photons per second (ph/s). Mice were subcutaneously injected with 500 μg d-Luciferin (PerkinElmer) and imaged 5 min later (Koyama et al., 2012).

RNA sequencing.

Total RNA was extracted from sort-purified IEC ($CD45^{neg}$ *Villin*-YFP^{+} $7AAD^{neg}$) from *Villin*Cre^{+}*Rosa26*YEP mice using the RNeasy mini kit (QIAGEN). For library preparation and sequencing, TruSeq Stranded Total RNA Ribo-Zero GOLD and NextSeq 75 cycle High output run (Illumina) were utilized, respectively. We compared IEC from naïve mice, those from mice 4 days after TBI but not transplanted, those from transplanted (BALB/c → *Villin*Cre^{+}*Rosa26*YFP) non-GVHD mice (i.e. transplanted with TCD grafts) and those from GVHD mice (transplanted with T cell replete grafts). Sequence reads were trimmed for adapter sequences using Cutadapt and aligned to the mm10 assembly using STAR aligner. The read counts per gene were estimated using RSEM and were utilized to determine differential gene expression between groups using Bioconductor package 'edgeR'. The default TMM normalization method of edgeR was used to normalise read counts between samples. Differentially expressed genes were considered significant if the Benjamini-Hochberg corrected p-value was less than 0.01. Gene set enrichment analysis (GSEA 3.0, Broad Institute) was used to determine gene sets and pathways that are significantly enriched in up and down differentially expressed genes (fold change > 2, fdr < 0.01) for each group of comparison against the GSEA molecular signature database. The gene sets that were significant with an FDR < 0.05 and are common in all comparisons from the above GSEA analysis were utilised for single-sample GSEA (ssGSEA) analysis. ssGSEA analysis reveals the pathways that are differentially regulated between the samples. The sample projection values for each pathway from ssGSEA analysis were used to construct a heat map demonstrating changes in pathway enrichments for each sample.

Statistical analysis.

Data were analysed using GraphPad Prism (ver. 7.02). Survival curves were plotted using Kaplan-Meier estimates and compared by log-rank test. If the equality of variance tests indicated the group variances were not significantly different ($p>0.01$) and the data was normally distributed, one-way ANOVA (Tukey's multiple comparison test) was used for multiple test comparisons or unpaired t-tests (two-tailed) for two group comparisons. For data that was not normally distributed, Kruskal-Wallis test (Dunn's multiple comparison test) was used for multiple group comparisons or Mann Whitney-U tests (two-tailed) for comparisons of two groups. When comparing in multiple ways, ANOVA or Kruskal-Wallis test was used for parametric and non-parametric comparisons respectively. Data are presented as mean ± standard error of the mean (SEM).

Supplementary Material

Refer to Web version on PubMed Central for supplementary material.

Acknowledgments

From QIMR Berghofer, we thank C. Winterford for expert preparation of histology samples, M. Rist, P. Hall and G. Chojnowski for expert cell sorting, M. Flynn for expert generation of the graphics and the animal facility for attentive animal care. We thank S. Robine (Institut Curie-CNRS, France) and R. S. Blumberg (Harvard Medical School, USA) for the *Villin*Cre-ER^{T2} mice.

Funding: This work was supported by research grants from the National Health and Medical Research Council (NHMRC). M.K. was funded for this project by grants from the Leukaemia Foundation of Australia and NHMRC (APP1086685). N.W. is a NHMRC Senior Research Fellow. M.A.D-E. is a NHMRC Principal Research Fellow. G.R.H. is a NHMRC Senior Principal Research Fellow. R.Z. is a Fellow of Deutsche Krebshilfe (RZ, no: 111639). B.R.B. is supported in part by National Institutes of Health Grants R37 AI34495.

References

Adolph TE, Tomczak MF, Niederreiter L, Ko HJ, Bock J, Martinez-Naves E, Glickman JN, Tschurtschenthaler M, Hartwig J, Hosomi S, et al. (2013). Paneth cells as a site of origin for intestinal inflammation. Nature 503, 272–276. [PubMed: 24089213]

Andermann TM, Peled JU, Ho C, Reddy P, Riches M, Storb R, Teshima T, van den Brink MRM, Alousi A, Balderman S, et al. (2018). The Microbiome and Hematopoietic Cell Transplantation: Past, Present, and Future. Biol Blood Marrow Transplant 24, 1322–1340. [PubMed: 29471034]

Beelen DW, Elmaagacli A, Muller KD, Hirche H, and Schaefer UW (1999). Influence of intestinal bacterial decontamination using metronidazole and ciprofloxacin or ciprofloxacin alone on the development of acute graft-versus-host disease after marrow transplantation in patients with hematologic malignancies: final results and long-term follow-up of an open-label prospective randomized trial. Blood 93, 3267–3275. [PubMed: 10233878]

Beilhack A, Schulz S, Baker J, Beilhack GF, Wieland CB, Herman EI, Baker EM, Cao YA, Contag CH, and Negrin RS (2005). In vivo analyses of early events in acute graft-versus-host disease reveal sequential infiltration of T-cell subsets. Blood 106, 1113–1122. [PubMed: 15855275]

Beura LK, Wijeyesinghe S, Thompson EA, Macchietto MG, Rosato PC, Pierson MJ, Schenkel JM, Mitchell JS, Vezys V, Fife BT, et al. (2018). T Cells in Nonlymphoid Tissues Give Rise to Lymph-Node-Resident Memory T Cells. Immunity 48, 327–338 e325. [PubMed: 29466758]

Biron CA, and Tarrio ML (2015). Immunoregulatory cytokine networks: 60 years of learning from murine cytomegalovirus. Med Microbiol Immunol 204, 345–354. [PubMed: 25850988]

Biton M, Haber AL, Rogel N, Burgin G, Beyaz S, Schnell A, Ashenberg O, Su CW, Smillie C, Shekhar K, et al. (2018). T Helper Cell Cytokines Modulate Intestinal Stem Cell Renewal and Differentiation. Cell 175, 1307–1320 e1322. [PubMed: 30392957]

Burman AC, Banovic T, Kuns RD, Clouston AD, Stanley AC, Morris ES, Rowe V, Bofinger H, Skoczylas R, Raffelt N, et al. (2007). IFNgamma differentially controls the development of idiopathic pneumonia syndrome and GVHD of the gastrointestinal tract. Blood 110, 1064–1072. [PubMed: 17449800]

Chang PV, Hao L, Offermanns S, and Medzhitov R (2014). The microbial metabolite butyrate regulates intestinal macrophage function via histone deacetylase inhibition. Proceedings of the National Academy of Sciences of the United States of America 111, 2247–2252. [PubMed: 24390544]

Cooke KR, Kobzik L, Martin TR, Brewer J, Delmonte J, Crawford JM, and Ferrara JLM (1996). An experimental model of idiopathic pneumonia syndrome after bone marrow transplantation. I. The roles of minor H antigens and endotoxin. Blood 88, 3230–3239. [PubMed: 8963063]

El Aidy S, van Baarlen P, Derrien M, Lindenbergh-Kortleve DJ, Hooiveld G, Levenez F, Dore J, Dekker J, Samsom JN, Nieuwenhuis EE, and Kleerebezem M (2012). Temporal and spatial interplay of microbiota and intestinal mucosa drive establishment of immune homeostasis in conventionalized mice. Mucosal immunology 5, 567–579. [PubMed: 22617837]

el Marjou F, Janssen KP, Chang BH, Li M, Hindie V, Chan L, Louvard D, Chambon P, Metzger D, and Robine S (2004). Tissue-specific and inducible Cre-mediated recombination in the gut epithelium. Genesis 39, 186–193. [PubMed: 15282745]

Feagan BG, Sandborn WJ, Gasink C, Jacobstein D, Lang Y, Friedman JR, Blank MA, Johanns J, Gao LL, Miao Y, et al. (2016). Ustekinumab as Induction and Maintenance Therapy for Crohn's Disease. N Engl J Med 375, 1946–1960. [PubMed: 27959607]

Ferrara JL, Levine JE, Reddy P, and Holler E (2009). Graft-versus-host disease. Lancet 373, 1550–1561. [PubMed: 19282026]

Hashimoto D, Chow A, Greter M, Saenger Y, Kwan WH, Leboeuf M, Ginhoux F, Ochando JC, Kunisaki Y, van Rooijen N, et al. (2011). Pretransplant CSF-1 therapy expands recipient macrophages and ameliorates GVHD after allogeneic hematopoietic cell transplantation. J Exp Med 208, 1069–1082. [PubMed: 21536742]

Hashimoto K, Joshi SK, and Koni PA (2002). A conditional null allele of the major histocompatibility IA-beta chain gene. Genesis 32, 152–153. [PubMed: 11857806]

Hayase E, Hashimoto D, Nakamura K, Noizat C, Ogasawara R, Takahashi S, Ohigashi H, Yokoi Y, Sugimoto R, Matsuoka S, et al. (2017). R-Spondin1 expands Paneth cells and prevents dysbiosis induced by graft-versus-host disease. J Exp Med 214, 3507–3518. [PubMed: 29066578]

Hill GR, and Ferrara JLM (2000). The primacy of the gastrointestinal tract as a target organ of graft-versus-host disease: Rationale for the use of cytokine shields in allogeneic bone marrow transplantation. Blood 95, 2754–2759. [PubMed: 10779417]

Hirota K, Duarte JH, Veldhoen M, Hornsby E, Li Y, Cua DJ, Ahlfors H, Wilhelm C, Tolaini M, Menzel U, et al. (2011). Fate mapping of IL-17-producing T cells in inflammatory responses. Nature immunology 12, 255–263. [PubMed: 21278737]

Hixon JA, Anver MR, Blazar BR, Panoskaltsis-Mortari A, Wiltrout RH, and Murphy WJ (2002). Administration of either anti-CD40 or interleukin-12 following lethal total body irradiation induces acute lethal toxicity affecting the gut. Biol Blood Marrow Transplant 8, 316–325. [PubMed: 12108917]

Hulsdunker J, Ottmuller KJ, Neeff HP, Koyama M, Gao Z, Thomas OS, Follo M, Al-Ahmad A, Prinz G, Duquesne S, et al. (2018). Neutrophils provide cellular communication between ileum and mesenteric lymph nodes at graft-versus-host disease onset. Blood 131, 1858–1869. [PubMed: 29463561]

Jenq RR, Ubeda C, Taur Y, Menezes CC, Khanin R, Dudakov JA, Liu C, West ML, Singer NV, Equinda MJ, et al. (2012). Regulation of intestinal inflammation by microbiota following allogeneic bone marrow transplantation. J Exp Med 209, 903–911. [PubMed: 22547653]

Johansson ME, Phillipson M, Petersson J, Velcich A, Holm L, and Hansson GC (2008). The inner of the two Muc2 mucin-dependent mucus layers in colon is devoid of bacteria. Proceedings of the National Academy of Sciences of the United States of America 105, 15064–15069. [PubMed: 18806221]

Kambayashi T, and Laufer TM (2014). Atypical MHC class II-expressing antigen-presenting cells: can anything replace a dendritic cell? Nat Rev Immunol 14, 719–730. [PubMed: 25324123]

Kennedy GA, Varelias A, Vuckovic S, Le Texier L, Gartlan KH, Zhang P, Thomas G, Anderson L, Boyle G, Cloonan N, et al. (2014). Addition of interleukin-6 inhibition with tocilizumab to standard graft-versus-host disease prophylaxis after allogeneic stem-cell transplantation: a phase 1/2 trial. Lancet Oncol 15, 1451–1459. [PubMed: 25456364]

Koyama M, Cheong M, Markey KA, Gartlan KH, Kuns RD, Locke KR, Lineburg KE, Teal BE, Leveque-El Mouttie L, Bunting MD, et al. (2015). Donor colonic CD103+ dendritic cells determine the severity of acute graft-versus-host disease. J Exp Med 212, 1303–1321. [PubMed: 26169940]

Koyama M, and Hill GR (2016). Alloantigen presentation and graft-versus-host disease: fuel for the fire. Blood 127, 2963–2970. [PubMed: 27030390]

Koyama M, Kuns RD, Olver SD, Raffelt NC, Wilson YA, Don AL, Lineburg KE, Cheong M, Robb RJ, Markey KA, et al. (2012). Recipient nonhematopoietic antigen-presenting cells are sufficient to induce lethal acute graft-versus-host disease. Nat Med 18, 135–142.

Lantz O, Grandjean I, Matzinger P, and Di Santo JP (2000). Gamma chain required for naive CD4+ T cell survival but not for antigen proliferation. Nature immunology 1, 54–58. [PubMed: 10881175]

Li H, Demetris AJ, McNiff J, Matte-Martone C, Tan HS, Rothstein DM, Lakkis FG, and Shlomchik WD (2012). Profound depletion of host conventional dendritic cells, plasmacytoid dendritic cells,

and B cells does not prevent graft-versus-host disease induction. Journal of immunology 188, 3804–3811.

Li H, Matte-Martone C, Tan HS, Venkatesan S, McNiff J, Demetris AJ, Jain D, Lakkis F, Rothstein D, and Shlomchik WD (2011). Graft-versus-host disease is independent of innate signaling pathways triggered by pathogens in host hematopoietic cells. Journal of immunology 186, 230–241.

Londei M, Lamb JR, Bottazzo GF, and Feldmann M (1984). Epithelial cells expressing aberrant MHC class II determinants can present antigen to cloned human T cells. Nature 312, 639–641. [PubMed: 6334239]

MacDonald KP, Palmer JS, Cronau S, Seppanen E, Olver S, Raffelt NC, Kuns R, Pettit AR, Clouston A, Wainwright B, et al. (2010). An antibody against the colony-stimulating factor 1 receptor depletes the resident subset of monocytes and tissue- and tumor-associated macrophages but does not inhibit inflammation. Blood 116, 3955–3963. [PubMed: 20682855]

Markey KA, Kuns RD, Browne DJ, Gartlan KH, Robb RJ, Martins JP, Henden AS, Minnie SA, Cheong M, Koyama M, et al. (2018). Flt-3L Expansion of Recipient CD8alpha(+) Dendritic Cells Deletes Alloreactive Donor T Cells and Represents an Alternative to Posttransplant Cyclophosphamide for the Prevention of GVHD. Clin Cancer Res 24, 1604–1616. [PubMed: 29367429]

Mathewson ND, Jenq R, Mathew AV, Koenigsknecht M, Hanash A, Toubai T, Oravecz-Wilson K, Wu SR, Sun Y, Rossi C, et al. (2016). Gut microbiome-derived metabolites modulate intestinal epithelial cell damage and mitigate graft-versus-host disease. Nature immunology 17, 505–513. [PubMed: 26998764]

McDonald GB, and Jewell DP (1987). Class II antigen (HLA-DR) expression by intestinal epithelial cells in inflammatory diseases of colon. J Clin Pathol 40, 312–317. [PubMed: 3558865]

Miyoshi H, and Stappenbeck TS (2013). In vitro expansion and genetic modification of gastrointestinal stem cells in spheroid culture. Nat Protoc 8, 2471–2482. [PubMed: 24232249]

Paludan C, Schmid D, Landthaler M, Vockerodt M, Kube D, Tuschl T, and Munz C (2005). Endogenous MHC class II processing of a viral nuclear antigen after autophagy. Science 307, 593–596. [PubMed: 15591165]

Pidala J, Beato F, Kim J, Betts B, Jim H, Sagatys E, Levine JE, Ferrara JLM, Ozbek U, Ayala E, et al. (2018). In vivo IL-12/IL-23p40 neutralization blocks Th1/Th17 response after allogeneic hematopoietic cell transplantation. Haematologica 103, 531–539. [PubMed: 29242294]

Roche PA, and Furuta K (2015). The ins and outs of MHC class II-mediated antigen processing and presentation. Nat Rev Immunol 15, 203–216. [PubMed: 25720354]

Rowe V, Banovic T, Macdonald KP, Kuns R, Don AL, Morris ES, Burman AC, Bofinger HM, Clouston AD, and Hill GR (2006). Host B cells produce IL-10 following TBI and attenuate acute GVHD after allogeneic bone marrow transplantation. Blood 107, 2485–2492.

Saada JI, Pinchuk IV, Barrera CA, Adegboyega PA, Suarez G, Mifflin RC, Di Mari JF, Reyes VE, and Powell DW (2006). Subepithelial myofibroblasts are novel nonprofessional APCs in the human colonic mucosa. Journal of immunology 177, 5968–5979.

Shan M, Gentile M, Yeiser JR, Walland AC, Bornstein VU, Chen K, He B, Cassis L, Bigas A, Cols M, et al. (2013). Mucus enhances gut homeostasis and oral tolerance by delivering immunoregulatory signals. Science 342, 447–453. [PubMed: 24072822]

Shlomchik WD, Couzens MS, Tang CB, McNiff J, Robert ME, Liu J, Shlomchik MJ, and Emerson SG (1999). Prevention of graft versus host disease by inactivation of host antigen- presenting cells. Science 285, 412–415. [PubMed: 10411505]

Shono Y, Docampo MD, Peled JU, Perobelli SM, Velardi E, Tsai JJ, Slingerland AE, Smith OM, Young LF, Gupta J, et al. (2016). Increased GVHD-related mortality with broad-spectrum antibiotic use after allogeneic hematopoietic stem cell transplantation in human patients and mice. Sci Transl Med 8, 339ra371.

Skoskiewicz MJ, Colvin RB, Schneeberger EE, and Russell PS (1985). Widespread and selective induction of major histocompatibility complex-determined antigens in vivo by gamma interferon. J Exp Med 162, 1645–1664. [PubMed: 3932581]

Stevanovic S, van Bergen CA, van Luxemburg-Heijs SA, van der Zouwen B, Jordanova ES, Kruisselbrink AB, van de Meent M, Harskamp JC, Claas FH, Marijt EW, et al. (2013). HLA class

II upregulation during viral infection leads to HLA-DP-directed graft-versus-host disease after CD4+ donor lymphocyte infusion. Blood 122, 1963–1973. [PubMed: 23777765]

Teshima T, Ordemann R, Reddy P, Gagin S, Liu C, Cooke KR, and Ferrara JL (2002). Acute graft-versus-host disease does not require alloantigen expression on host epithelium. Nat Med 8, 575–581. [PubMed: 12042807]

Thelemann C, Eren RO, Coutaz M, Brasseit J, Bouzourene H, Rosa M, Duval A, Lavanchy C, Mack V, Mueller C, et al. (2014). Interferon-gamma induces expression of MHC class II on intestinal epithelial cells and protects mice from colitis. PloS one 9, e86844. [PubMed: 24489792]

Toubai T, Tawara I, Sun Y, Liu C, Nieves E, Evers R, Friedman T, Korngold R, and Reddy P (2012). Induction of acute GVHD by sex-mismatched H-Y antigens in the absence of functional radiosensitive host hematopoietic-derived antigen-presenting cells. Blood 119, 3844–3853. [PubMed: 22101894]

Unanue ER, Turk V, and Neefjes J (2016). Variations in MHC Class II Antigen Processing and Presentation in Health and Disease. Annu Rev Immunol 34, 265–297. [PubMed: 26907214]

Varelias A, Gartlan KH, Kreijveld E, Olver SD, Lor M, Kuns RD, Lineburg KE, Teal BE, Raffelt NC, Cheong M, et al. (2015). Lung parenchyma-derived IL-6 promotes IL-17A-dependent acute lung injury after allogeneic stem cell transplantation. Blood 125, 2435–2444. [PubMed: 25673640]

Varelias A, Ormerod KL, Bunting MD, Koyama M, Gartlan KH, Kuns RD, Lachner N, Locke KR, Lim CY, Henden AS, et al. (2017). Acute graft-versus-host disease is regulated by an IL-17-sensitive microbiome. Blood 129, 2172–2185. [PubMed: 28137828]

Vatanen T, Kostic AD, d'Hennezel E, Siljander H, Franzosa EA, Yassour M, Kolde R, Vlamakis H, Arthur TD, Hamalainen AM, et al. (2016). Variation in Microbiome LPS Immunogenicity Contributes to Autoimmunity in Humans. Cell 165, 842–853. [PubMed: 27133167]

Vossen JM, Heidt PJ, van den Berg H, Gerritsen EJ, Hermans J, and Dooren LJ (1990). Prevention of infection and graft-versus-host disease by suppression of intestinal microflora in children treated with allogeneic bone marrow transplantation. Eur J Clin Microbiol Infect Dis 9, 14–23. [PubMed: 2105890]

Weizman OE, Adams NM, Schuster IS, Krishna C, Pritykin Y, Lau C, Degli-Esposti MA, Leslie CS, Sun JC, and O'Sullivan TE (2017). ILC1 Confer Early Host Protection at Initial Sites of Viral Infection. Cell 171, 795–808 e712. [PubMed: 29056343]

Yamamoto M, Sato S, Hemmi H, Hoshino K, Kaisho T, Sanjo H, Takeuchi O, Sugiyama M, Okabe M, Takeda K, and Akira S (2003). Role of adaptor TRIF in the MyD88-independent toll-like receptor signaling pathway. Science 301, 640–643. [PubMed: 12855817]

Zeiser R, and Blazar BR (2017). Acute Graft-versus-Host Disease - Biologic Process, Prevention, and Therapy. N Engl J Med 377, 2167–2179. [PubMed: 29171820]

Zhang P, Lee JS, Gartlan KH, Schuster IS, Comerford I, Varelias A, Ullah MA, Vuckovic S, Koyama M, Kuns RD, et al. (2017). Eomesodermin promotes the development of type 1 regulatory T (TR1) cells. Sci Immunol 2, eaah7152. [PubMed: 28738016]

Highlights

- The microbiota influences MHC-II expression on IEC in the ileum
- MHC-II expression on IEC requires an IL-12-IFNγ cytokine axis
- MHC-II^{+} IEC present antigen, activate CD4^{+} T cells and initiate lethal gut GVHD
- IL-12/23p40 neutralization pre-transplant prevents the initiation of lethal GVHD

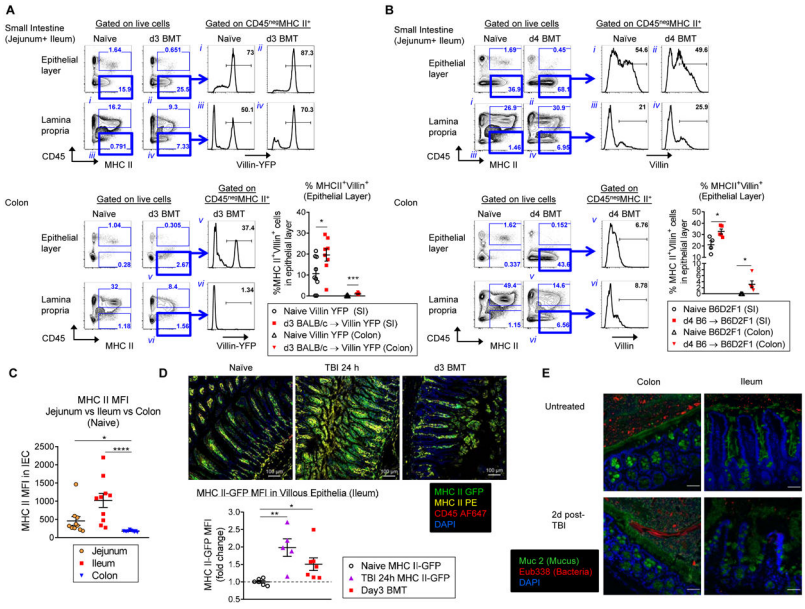

Figure 1. IEC in the ileum express MHC-II and MHC-II expression increases after TBI.

(**A, B**) MHC-II expression in the small (pooled jejunum and ileum) and large intestine was analyzed in naïve and transplanted mice. Representative flow plots and enumeration are shown.

(**A**) Lethally irradiated *Villin*Cre^{pos}*Rosa26*-YFP mice were transplanted with BM and T cells from BALB/c mice and analysed on day 3 (*d*3) post-transplant. Data combined from 3 replicate experiments ($n = 9$ per group).

(**B**) Irradiated B6D2F1 mice were transplanted with BM and T cells from B6.WT mice and analysed on *d*4. Data combined from 2 replicate experiments ($n = 4 – 5$ per group). (**C**) MHC-II expression (MFI) was quantified on IEC (EpCAM$^+$ CD45^{neg}) of the jejunum, ileum and colon from naïve B6.WT mice, combined from 2 replicate experiments ($n = 10$ per group).

(**D**) Naïve B6.*I-A*^{b}*β*-GFP mice, 24 hours (24*h*) after TBI or *d*3 after BMT with BM and T cells from BALB/c mice as in (A). Immunofluorescence (green = MHC-II-GFP; yellow = MHC-II (anti-IA/IE Ab staining); red = CD45; blue = DAPI). Representative images and standardized enumeration combined from 3 replicate experiments ($n = 5 – 6$ per group).

(**E**) Immunofluorescence staining of colonic and ileal tissue of naive B6 mice and at 2*d* post-TBI. Bidirectional arrows indicate the colon's inner mucous layer which is free from bacteria. [Muc2 = green, eubacterial probe (Eub338) = red, DAPI = blue, scale bar = 50 μm]. Statistical analysis by unpaired t-test per organ (A), Mann-Whitney U test per organ (B) or Kruskal-Wallis test (C, D) (mean ± SEM). *$P < 0.05$, ** $P < 0.01$, *** $P < 0.001$. See also Figure S1.

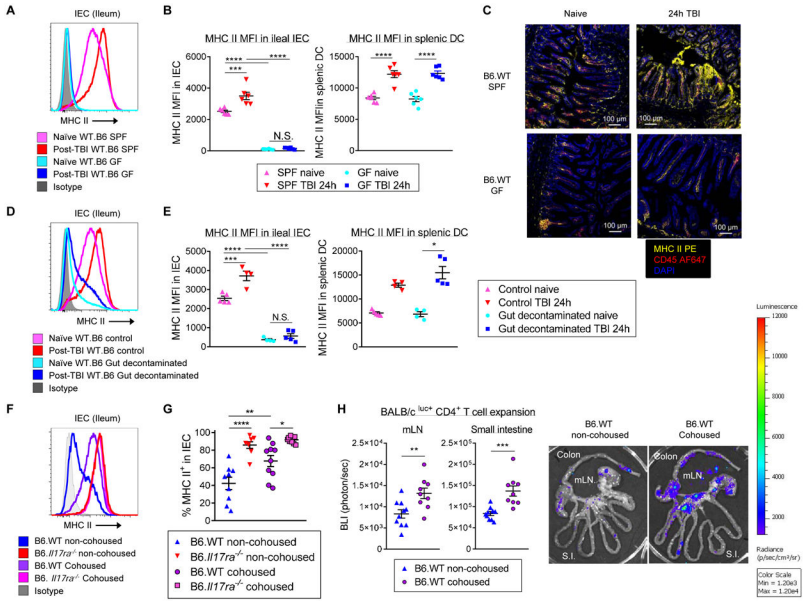

Figure 2. The intestinal microbiota is required for MHC-II expression on IEC pre-transplant.

(**A-C**) (**A**) Representative histograms of MHC-II on ileal IEC ($EpCAM^{+}CD45^{neg}$) purified from specific pathogen free (SPF) and germ free (GF) mice before (naïve) and 24*h* after TBI, (**B**) MHC-II MFI on IEC and splenic DC ($CD45^{+}CD3^{neg}CD19^{neg}NK1.1^{neg}Ly6C^{neg}Ly6G^{neg}CD11c^{+}CD64^{neg}$) ($n = 6$ per group from 3 experiments), (**C**) Confocal images from the ileum. (**D, E**) (**D**) Representative histograms of MHC-II on IEC in the ileum of mice treated with antibiotic water or control water for 2 weeks and analyzed before (naïve) and 24*h* after TBI, (**E**) MHC-II MFI on IEC and splenic DC ($n = 4 – 5$ per group from 2 replicate experiments). (**F, G**) B6.WT and B6.*Il17ra*$^{-/-}$ mice were housed separately or cohoused for 6 weeks. (**F**) Representative histograms of MHC-II on IEC and (**G**) frequency of MHC-II^{+} IEC ($n = 8 – 10$ per group combined from 2 replicate experiments). (**H**) Cohoused or individually housed B6.WT mice were transplanted with $CD4^{+}$ T cells from BALB/c^{luc+} mice. Quantification and representative images of *d7* bioluminescence (BLI) data (allogeneic $CD4^{+}$ T cell expansion) combined from 2 replicate experiments ($n = 9 – 10$ per group) are shown. Statistical analysis by unpaired t-test (**H**), ANOVA (ileum and spleen in **B**, ileum in **E** and **G**) and Kruskal-Wallis test (spleen in **E**) (mean ± SEM). *$P < 0.05$, ** $P < 0.01$, *** $P < 0.001$, ****$P < 0.0001$. See also Figure S1.

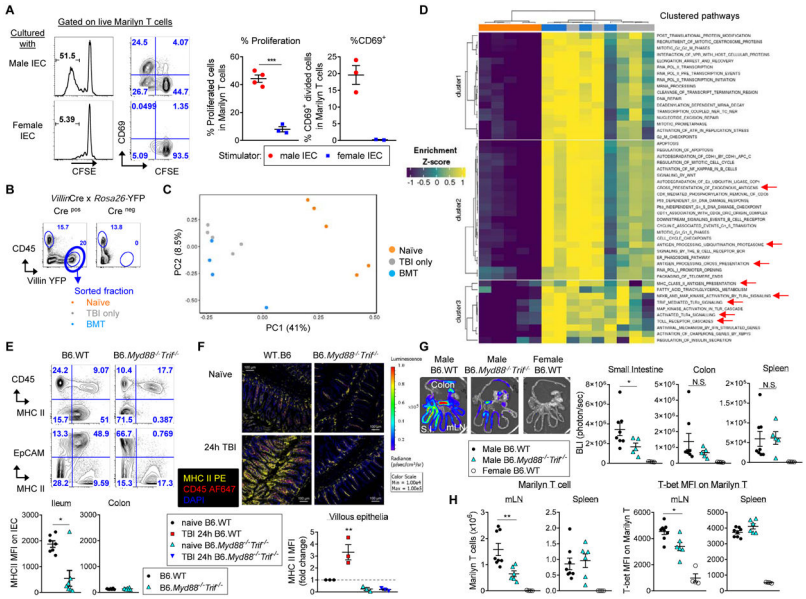

Figure 3. MyD88 and TRIF signalling are necessary for MHC-II expression by IEC in the ileum pre-transplant.

(**A**) Mixed Lymphocyte Reaction (MLR) of CFSE-labelled sort-purified HY-reactive Marilyn CD4^{+} T cells co-cultured with sort-purified 7AAD^{neg} EpCAM^{+} CD45^{neg} IEC from the small intestine of irradiated male (HY-positive) or female (HY-negative) mice, analysed at *d7*. Data are representative of 3 replicate experiments ($n = 3 – 4$). (**B**) Epithelial cells from the small intestine (7AAD^{neg}Villin^{+}CD45^{neg}) of naïve *Villin*Cre^{pos}*Rosa26*-YFP mice, those 4*d* post-TBI or 3*d* post-BMT were sort-purified and processed for RNAseq gene expression analysis ($n = 4 – 5$ per group). (**C**) First and second principal component projections. (**D**) Clustered heat map of the top 50 gene-sets that significantly differentially increased at FDR < 0.05 between groups of samples analysed using ssGSEA. (**E**) Representative flow plots and MFI of MHC-II expression in the epithelial fractions from naïve B6.WT and B6.*Myd88*$^{-/-}$*Trif*$^{-/-}$ mice. Data combined from 2 replicate experiments ($n = 7$ per group). (**F**) Representative confocal images of MHC-II expression on ileum before and 24*h* after TBI with quantification normalized to naïve WT mice ($n = 3$ per group). (**G-H**) Male B6.WT and B6.*Myd88*$^{-/-}$*Trif*$^{-/-}$ mice were transplanted with Marilyn^{luc+} T cells and analyzed on *d7*. WT female recipients were utilized as negative controls ($n = 4$). (**G**) Representative BLI images and signal quantification in small intestine, colon and spleen are shown. (**H**) Marilyn $^{luc+}$ T cell quantification and T-bet expression in mLN and spleen. ($n =$ 5 – 8 per male group combined from 2 replicate experiments). Statistical analysis by unpaired t-test (**A**), Mann-Whitney U test (**E,G,H**) or ANOVA (**F**) (mean ± SEM). *$P <$ 0.05, ** $P < 0.01$, *** $P < 0.001$. See also Figure S2 -4.

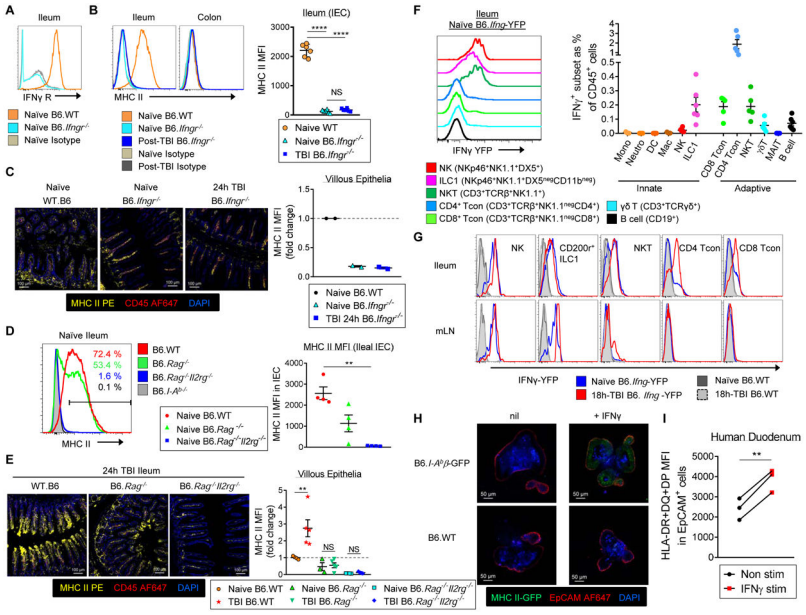

Figure 4. IFNγ drives MHC-II expression on IEC.

Representative (**A**) IFNγR and (**B**) MHC-II expression on IEC (7AAD^{neg}EpCAM^{+}CD45^{neg}) from naïve and 24*h* post-TBI, B6.WT and B6.*Ifngr*$^{-/-}$ mice. Quantified data shown (right) is combined from 3 replicate experiments ($n = 6$ per group). (**C**) Fluorescence images of ileum from B6.*Ifngr*$^{-/-}$ (naïve and 24*h* post-TBI) and B6.WT (naïve) mice. Representative images and quantification from 2 replicate experiments. (**D**) Representative MHC-II expression on IEC from naïve B6.WT, B6.*Rag*$^{-/-}$, B6. *Rag*$^{-/-}$*Il2rg*$^{-/-}$ and B6.*I-A*$^{b-/-}$ mice. Quantification shown right ($n = 4$ per group from 3 experiments). (**E**) Fluorescence images of ileum from 24*h* post-TBI of B6.WT, B6.*Rag*$^{-/-}$ and B6.*Rag*$^{-/-}$*Il2rg*$^{-/-}$ mice. Representative images (left) and quantification from 2 replicate experiments are shown ($n = 3 – 5$ per group). (**F**) Representative IFNγ-YFP expression (left) and quantified data (right) in hematopoietic cell subsets within the ileum from naïve mice are shown ($n = 3 – 6$ per group from 3 replicate experiments). (**G**) IFNγ-YFP expression shown in the indicated populations from the ileum and mLN of naïve mice and 18*h* after TBI. (**H**) Representative confocal images of small intestinal organoids generated from B6. *I-A*^{b}*β*-GFP or B6.WT mice in the presence or absence of IFNγ. Representative images from 2 replicate experiments. (**I**) Flow cytometric quantification of HLA class-II MFI in 7AAD^{neg}EpCAM^{+}CD45^{neg} cells from human duodenum organoids before and after IFNγ stimulation (healthy donors, $n = 3$, paired t-test). Multiple comparisons by ANOVA (**B, E**) or Kruskal-Wallis test (**D**) (mean ± SEM). *$P < 0.05$, ** $P < 0.01$, **** $P < 0.0001$. See also Figure S5.

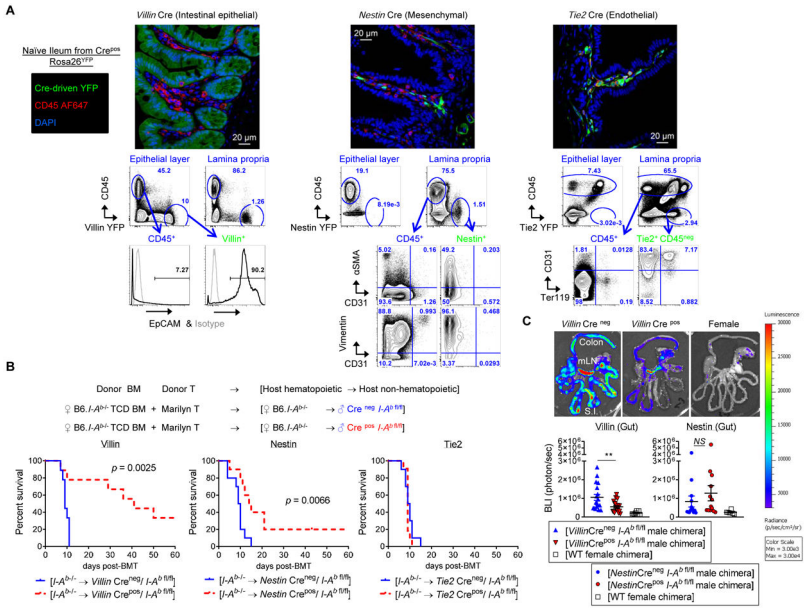

Figure 5. IEC induce MHC-II-dependent GVHD.

(**A**) The distribution (top: confocal images) and lineage (bottom: flow cytometry) of YFP^{+} cells in the ileum from naïve *Villin*Cre^{pos}*Rosa26*-YFP, *Nestin*Cre^{pos}*Rosa26*-YFP or *Tie2*Cre^{pos}*Rosa26*-YFP mice. Representative of two replicate experiments. (**B**) B6 male *Nestin*, *Villin* or *Tie2* Cre^{pos}*I-A*$^{b\text{-}fl/fl}$ mice and relevant Cre^{neg}*I-A*$^{b\text{-}fl/fl}$ mice were transplanted with BM from female B6.*I-A*$^{b-/-}$ mice. 3 months later, these chimeric mice were transplanted with BM from female B6.*I-A*$^{b-/-}$ mice and 25 × 10^{3} sorted Marilyn T cells. Survival by Kaplan-Meier analysis, combined from 2 replicate experiments (n = 9 – 11 per group). P = 0.0025 (*Villin*), 0.0066 (*Nestin*): Cre ^{pos}*I-A*$^{b\text{-}fl/fl}$ vs. Cre ^{neg}*I-A*$^{b\text{-}fl/fl}$ chimeric recipients. (**C**) BM chimeric recipients were transplanted as in (B), but with 0.2 × 10^{6} sorted Marilyn^{luc+} T cells. Representative BLI images and quantitative data on d7 combined from 3 – 4 replicate experiments are shown (n = 12 – 21 per group). Two-tailed unpaired t test (mean ± SEM), ** P = 0.0090, N.S. = not significant. See also Figure S6.

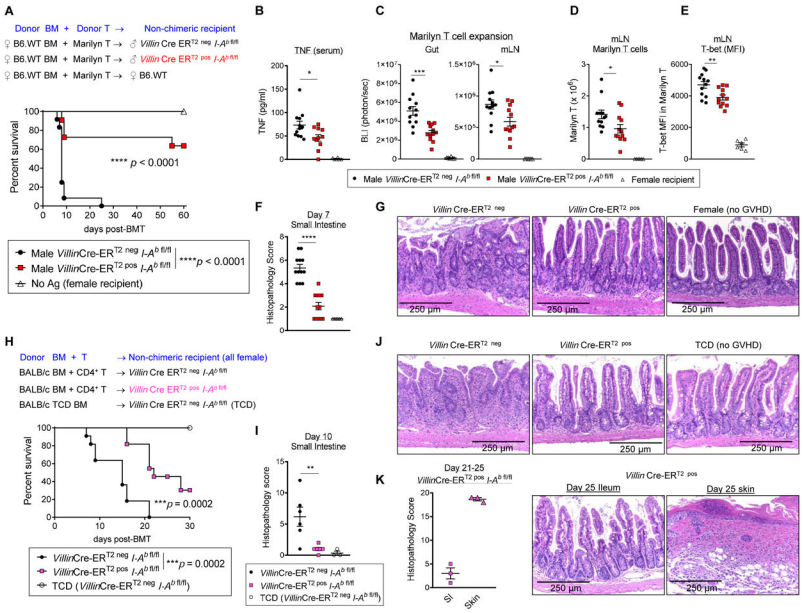

Figure 6. MHC-II-expressing IEC elicit alloantigen reactive T cell expansion and Th1 differentiation in the GI tract.

Male (**A** – **G**) or female (**H** – **K**) *Villin* Cre-ER$^{T2\text{-}neg}$*I-A*$^{b\text{-}fl/fl}$ and Cre-ER$^{T2\text{-}pos}$*I-A*$^{b\text{-}fl/fl}$ or female B6.WT mice (**A** – **G**) were treated with Tamoxifen 2 weeks before transplant. (**A**) Tamoxifen-treated mice were transplanted with B6.WT BM with 0.5 × 10^6 CD4 MACS-purified Marilyn T cells. Female recipients are negative controls. Survival by Kaplan-Meier analysis, combined from 2 replicate experiments (n = 11 – 12 per T cell replete group). (**B** – **G**) Recipients were transplanted as in (A) but with 0.2 × 10^6 sorted Marilyn $^{luc+}$ T cells. Serum TNF, BLI data, enumeration of Marilyn T cells with MFI of T-bet expression and intestinal histology on d7 are shown, combined from 3 replicate experiments (n = 12 per T cell replete group). (**H** – **K**) Lethally irradiated Tamoxifen-treated female mice were transplanted with BM and T_{reg}-depleted $CD4^+$ T cells from PC61-treated BALB/c mice. (**H**) Survival by Kaplan-Meier analysis, combined from 2 replicate experiments (n = 11 per T cell replete group); (**I, J**) Intestinal histopathology scores on d10 (n = 6 per T cell replete group); and (**K**) late skin histology (n = 3). *P < 0.05; **P < 0.01; ***P < 0.001; ****P < 0.0001: *Villin* Cre-ER$^{T2\text{-}neg}$*I-A*$^{b\text{-}fl/fl}$ vs. Cre-ER$^{T2\text{-}pos}$*I-A*$^{b\text{-}fl/fl}$. Statistical analysis by two-tailed Mann-Whitney U test (**B - F**) or t-test (**I**) (mean ± SEM), except for survival data. See also Figure S6 - 7.

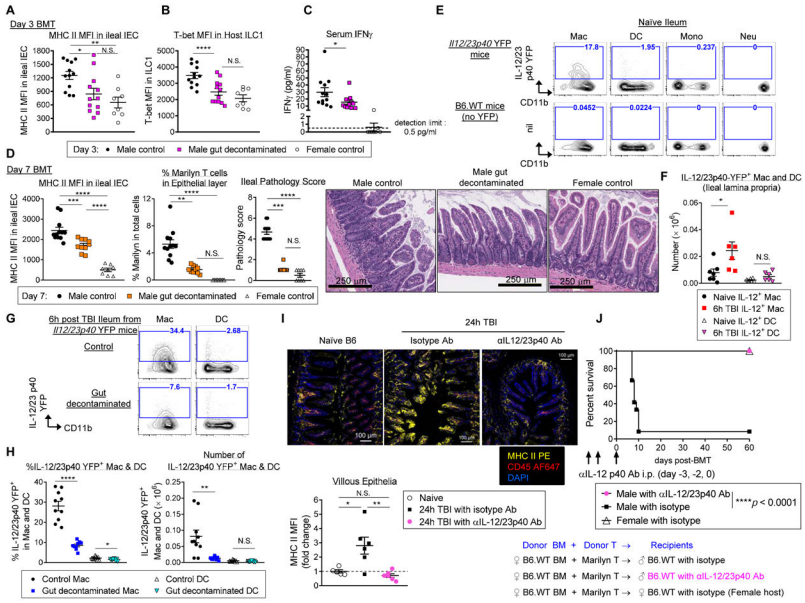

Figure 7. Neutralizing IL-12 prior to irradiation prevents the induction of MHC-II expression on IEC pre-transplant and subsequent GVHD.

B6.WT mice (**A – D**) and B6.*Il12/23p40*-YFP mice (**G, H**) received either antibiotic water or normal water for 2 weeks. (**A - D**) Lethally irradiated male B6.WT gut decontaminated mice and control male and female mice were transplanted with 0.2×10^6 Marilyn T cells. (**A - C**) Ileum was analysed on *d*3. (**A**) MHC-II expression quantified on IEC (EpCAM $^{+}$CD45^{neg}), (**B**) T-bet MFI in host ILC1 and (**C**) serum IFNγ ($n = 8 – 12$ per group from 2 replicate experiments, Mann Whitney U test). (**D**) Quantification of MHC-II expression on IEC (left), frequency of Marilyn T cells infiltrating the epithelial fraction (middle) and ileum GVHD histopathology scores (right) with representative H&E stained images on *d*7 are shown ($n = 8 – 12$ per group from 2 replicate experiments). (**E**) Representative flow plots of IL-12/23p40-YFP expression on macrophages (Mac), DC, monocytes (Mono) and neutrophil (Neu) from naïve B6.*Il12/23p40*-YFP mice (from 3 replicate experiments). B6.WT mice were gated as negative controls. (**F**) Quantification of *Il12/23p40*-YYP^{+} Mac and DC from naïve mice or 6*h* post-TBI ($n = 6 – 7$ per group from 3 replicate experiments, unpaired t-test). (**G, H**) Representative flow plots (**G**) and frequency (left) and numbers (right) of IL-12/23p40-YFP^{+} cells (**H**) in the ileum of mice 24*h* after TBI ($n = 9 – 10$ per group from 2 replicate experiments, unpaired t-test). (**I**) B6.WT mice were treated with IL-12/23p40 mAb or isotype control at 48*h* and 24*h* prior to TBI. Representative ileal image are shown with quantification ($n = 5 – 6$ per group from 2 replicate experiments). (**J**) Survival by Kaplan-Meier estimates. Male B6.WT mice were treated with IL-12/23p40 mAb or isotype control at 48*h* (*d*-3), 24*h* (*d* −2) prior to TBI and *d* 0 prior to the infusion of B6.WT BM and Marilyn T cells ($n = 12$, combined from 2 replicate experiments). Female recipients ($n = 4$) were used as negative controls. Multiple comparisons by ANOVA, except **D** (ileal pathology), Kruskal-Wallis test, (mean ± SEM). *$P < 0.05$, ** $P < 0.01$, **** $P < 0.0001$. See also Figure S7.

KEY RESOURCES TABLE

REAGENT or RESOURCE	SOURCE	IDENTIFIER
Antibodies		
Alexa Fluor 700 anti-mouse CD45.2	BioLegend	Cat# 109822, RRID AB_493731
FITC anti-mouse CD45.2	BioLegend	Cat# 109806, RRID AB_313443
PE anti-mouse CD31	BioLegend	Cat# 102408, RRID AB_312903
APC anti-mouse TER-119	BioLegend	Cat# 116212, RRID AB_313713
Pacific Blue anti-mouse I-A/I-E	BioLegend	Cat# 107620, RRID AB_493527
Pacific Blue anti-mouse CD69	BioLegend	Cat# 104524, RRID AB_2074979
Alexa Fluor 647 anti-mouse CD326 (EpCAM)	BioLegend	Cat# 118212, RRID AB_1134101
PE-CF594 Rat Anti-Mouse CD19	BD Biosciences	Cat# 562291, RRID AB_11154223
BV650 Hamster Anti-Mouse CD3	BD Biosciences	Cat# 564378, RRID AB_2738779
BV711 Hamster Anti-Mouse CD3	BD Biosciences	Cat# 563123, RRID AB_2687954
PerCP/Cyanine5.5 anti-mouse TCRβ	BioLegend	Cat# 109228, RRID AB_1575173
Brilliant Violet 421 ™ anti-mouse TCRγδ	BioLegend	Cat# 118119, RRID AB_10896753
PerCP-Cy™5.5 Rat Anti-Mouse CD4	BD Biosciences	Cat# 550944, RRID AB_393977
BV711 Rat Anti-Mouse CD8a	BioLegend	Cat# 563046, RRID AB_2737972
PE/Cy7 anti-mouse CD335 (NKp46)	BioLegend	Cat# 137618, RRID AB_11219186
APC/Cy7 anti-mouse Ly-6G	BioLegend	Cat# 127624, RRID AB_10640819
Brilliant Violet 605 anti-mouse CD11c	BioLegend	Cat# 117334, RRID AB_2562415
PE/Cy7 anti-mouse CD64 (FcγRI)	BioLegend	Cat# 139314, RRID AB_2563904
PerCP/Cyanine5.5 anti-mouse/human CD11b	BioLegend	Cat# 101228, RRID AB_893232
PE anti-mouse CD40	BioLegend	Cat# 124610, RRID AB_1134075
PE anti-mouse CD80	BioLegend	Cat# 104708, RRID AB_313129
PE anti-mouse CD86	BioLegend	Cat# 105008, RRID AB_313151
PE Rat IgG2a, κ Isotype control	BioLegend	Cat# 400508, RRID AB_326530
PE Armenian Hamster IgG Isotype control	BioLegend	Cat# 400908, RRID AB_326593
Pacific Blue Rat IgG2b, κ Isotype control	BioLegend	Cat# 400627, RRID AB_493561
Alexa Fluor 647 anti-T-bet	BioLegend	Cat# 644804, RRID AB_1595466
Alexa Fluor 647 Mouse IgG1, κ Isotype control	BioLegend	Cat# 400136
CD90.1 Monoclonal Antibody (HIS51), APC-eFluor 780	eBioscience	Cat# 47-0900-82, RRID AB_1272252
CD200 Receptor Monoclonal Antibody (OX110), APC	eBioscience	Cat# 17-5201-82, RRID AB_10717289
APC Rat IgG2a, κ Isotype control	BioLegend	Cat# 400512
FITC Rat Anti-Mouse Vβ 6 T-Cell Receptor	BD Biosciences	Cat# 553193, RRID AB_394700
Biotin Rat Anti-Mouse CD49b (DX5)	BD Biosciences	Cat# 553856, RRID AB_395092
BV421 Mouse Anti-Mouse NK1.1	BD Biosciences	Cat# 562921, RRID AB_2728688
Alexa Fluor® 700 anti-mouse Ly-6C	BD Biosciences	Cat# 128024, RRID AB_10643270
CD119 (IFN γ Receptor 1) Monoclonal Antibody (2E2), PE	BD Biosciences	Cat# 12-1191-82, RRID AB_1210730
BV786 Streptavidin	BD Biosciences	Cat# 563858

REAGENT or RESOURCE	SOURCE	IDENTIFIER
Recombinant Anti-Villin antibody [SP145]	Abcam	Cat# ab130751
Rabbit IgG, monoclonal [EPR25A] - Isotype Control	Abcam	Cat# ab172730
Goat Anti-Rabbit IgG H&L (Alexa Fluor® 555)	Abcam	Cat# ab150086
Alexa Fluor 647 Rabbit monoclonal Anti-Vimentin antibody [EPR3776]	Abcam	Cat# ab194719
Alexa Fluor 647-Rabbit IgG, monoclonal [EPR25A] - Isotype Control	Abcam	Cat# ab199093
Anti-Alpha-Smooth Muscle Actin eFluor 660	eBioscience	Cat# 50-9760
Mouse IgG2a, K Isotype Control eFluor 660	eBioscience	Cat# 50-4727
LIVE/DEAD™ Fixable Aqua Dead Cell Stain Kit	ThermoFisher	Cat# L34957
Alexa Fluor® 647 anti-mouse CD45	BioLegend	Cat# 103124, RRID AB_493533
Alexa Fluor® 647 Rat IgG2b, κ Isotype control	BioLegend	Cat# 400626, RRID AB_389343
PE anti-mouse I-A/I-E	BioLegend	Cat# 107608, RRID AB_313323
PE Rat IgG2b, κ Isotype control	BioLegend	Cat# 400636, RRID AB_893669
Anti-HLA DR+DP+DQ antibody [WR18] PE	Abcam	Cat# Ab23901
PE Mouse IgG2a, κ Isotype control	BioLegend	Cat# 400244
Alexa Fluor 647 anti-human CD45	BioLegend	Cat# 304018, RRID AB_389336
Alexa Fluor 647 Mouse IgG1, κ Isotype control	BioLegend	Cat# 400130, RRID AB_2800436
Alexa Fluor 488 anti-human CD326 (EpCAM)	BioLegend	Cat# 324210, RRID AB_756084
Alexa Fluor 488 Mouse IgG2b, k isotype control	BioLegend	Cat# 400329
LEAF™ Purified anti-mouse CD80	BioLegend	Cat# 104710, RRID AB_313131
Ultra-LEAF™ Purified Armenian Hamster IgG Isotype control	BioLegend	Cat# 400940, RRID AB_11203529
Purified CD4 (clone GK1.5)	ATCC	TIB-207
Purified CD8β (clone 53-5.8)	QIMR Berghofer	N/A
Purified CD25 (clone PC-61.5.3)	ATCC	TIB-222
Bacterial and Virus Strains		
N/A		
Biological Samples		
Human duodenal tissue from healthy donors	Mater Inflammatory Bowel Disease (IBD) Biobank, Mater Research Institute	N/A
Chemicals, Peptides, and Recombinant Proteins		
Recombinant Human IFN-γ	BioLegend	Cat# 570204

REAGENT or RESOURCE	SOURCE	IDENTIFIER
D-Luciferin	Perkin Elmer	Cat# 122799
Recombinant Human IL-2 (Proleukin)	Novartis	
7-Aminoactinomycin D (7AAD)	Sigma Aldrich	Cat# A9400-5MG
Phorbol 12-myristate 13-acetate (PMA)	Sigma Aldrich	Cat#P1585-1MG
Ionomycin	Sigma Aldrich	Cat#I0634-1MG
Brefeldin A Solution (1000X)	BioLegend	Cat#420601
Carboxyfluorescein succinimidyl ester (CFSE)	Sigma Aldrich	Cat#21888-25MG-F
Cultex PathClear Reduced Growth Factor BME	R&D Systems	Cat#RDS353301002
SB431542	Selleck Chemicals	Cat#S1067-50mg
Y-27532 dihydrochloride	Tocris Bioscience	Cat#RDS125410
G418 disulfate salt solution	Sigma Aldrich	Cat#G8168-10ML
Hygromycin B Gold	Invivogen	Cat#ant-hg-1
Ethylenediaminetetraacetic Acid Disodium	Chem-supply	CAS#6381-92-6
Trypsin 2.5%	Thermo Fisher	Cat#15090-046
Tamoxifen	MP Biomedicals	CAS#10540-29-1
Critical Commercial Assays		
BD Cytofix/Cytoperm™ Fixation/Permeabilization Kit	BD Biosciences	Cat# 554714
eBioscience™ Foxp3 / Transcription Factor Staining Buffer Set	eBioscience	Cat# 00-5523-00
Cytometric Bead Array; IFNγ, IL-6, TNF, IL-17A	BD Biosciences	Cat#560485
Lamina Propria Dissociation Kit, mouse	MACS Miltenyi Biotec	Cat#130-097-410
RNeasy Mini Kit	QIAGEN	Cat# 74106
TruSeq Stranded Total RNA Ribo-Zero GOLD	Illumina	Cat#RS-122
NextSeq 75 cycle High output run	Illumina	Cat#FC-404-1005
Deposited Data		
Raw RNAseq data	European Nucleotide Archive	PRJEB33777, https://www.ebi.ac.uk/ena
Experimental Models: Cell Lines		
L-WRN (ATCC CRL-3276)	ATCC	Cat#CRL-3276; RRID:CVCL_DA06
Experimental Models: Organisms/Strains (mouse)		
Mouse: B6.WT : C57BL/6JArc	The Animal Resources Centre (ARC), Perth, AU	

REAGENT or RESOURCE	SOURCE	IDENTIFIER
Mouse: BALB/c: BALB/cArc	ARC	
Mouse: B6D2F1: B6D2F1J/Arc	ARC	
Mouse: B6.*Rag*$^{-/-}$: *Rag1*$^{-/-}$	QIMR Berghofer	
Mouse: B6.*Rag*$^{-/-}$ *Il2rg*$^{-/-}$: *Rag2*$^{-/-}$ *Il2rg*$^{-/-}$	QIMR Berghofer	
Mouse: B6.*I-A*$^{b-/-}$: *H2-Ab*$^{-/-}$	Australian National University, Canberra, AU	Grusby M.J., et al. 1991
Mouse: *Villin* Cre-ER^{T2}	Dr R Blumberg, Harvard Medical School, Boston, MA, USA	El Marjou F., et al. 2004
Mouse: *Rosa26*-YFP	Dr B. Stockinger, MRC National Institute for Medical Research, Mill Hill, London, UK	Srinivas, S. et al. 2001
Mouse: B6 $^{luc+:}$ *β-actin*-luciferase C57BL6J	Dr Robert Negrin, Stanford, CA, USA	
Mouse: BALB/c $^{luc+:}$ *β-actin*-luciferase BALB/c	Dr Robert Negrin, Stanford, CA, USA	
Mouse: Marilyn Tg (*Rag2*$^{-/-}$ background)	Dr P Matzinger, NIH, Bethesda, MD, USA	
Mouse: B6.*I-A*^{b}*β*-GFP: *I-A*^{b}*β*-EGFP	Dr Barbara Fazekas de St Groth, Garvan Institute, Sydney, AU	Boes, M. et al. 2002
Mouse: B6.*Myd88*$^{-/-}$ *Trif*$^{-/-}$	Dr S Akira, Osaka University, Osaka, Japan	
Mouse: B6.*il17ra*$^{-/-}$: *il17ra*$^{-/-}$	Amgen	
Mouse: *I-A*$^{b\text{-}fl/fl}$: B6.129X1-*H2-Ab1tm1Koni*/J	The Jackson Laboratory	013081
Mouse: *Villin*-Cre: B6.SJL-*Tg(Vil-cre)997Gum*/J	The Jackson Laboratory	004586
Mouse: *Nestin*-Cre: B6.Cg-*Tg(Nes-cre)1Kln*/J	The Jackson Laboratory	003771
Mouse: *Tie2*-Cre: B6.Cg-*Tg(Tek-cre)1Ywa*/J	The Jackson Laboratory	008863
Mouse: B6.*Il12/23p40*-YFP: B6.129-*Il12btm1Lky*/J	The Jackson Laboratory	006412
Mouse: B6.*Ifnγ*-YFP: B6.129S4-*Ifngtm3.1Lky*/J	The Jackson Laboratory	017581
Mouse: B6.*Ifngr*$^{-/-}$: B6.129S7-*Ifngr1tm1Agt*/J	The Jackson Laboratory	003288
Mouse: B6.*Il12p35*$^{-/-}$: B6.129S1-*Il12atm1Jm*/J	The Jackson Laboratory	002692
Mouse: Marilyn^{luc+}: *Rag2*$^{-/-}$ Marilyn mice were backcrossed onto a B6 β-actin-luciferase background	QIMR Berghofer	
Each of the Cre strain and I-A$^{b\text{-}fl/fl}$ or *Rosa26*-YFP strains were intercrossed to generate:		
Mouse: *Villin*-Cre $^{I\text{-}Ab\text{-}fl/fl}$	QIMR Berghofer	
Mouse: *Villin*-Cre-ER^{T2} *I-A*$^{b\text{-}fl/fl}$	QIMR Berghofer	
Mouse: *Nestin*-Cre *I-A*$^{b\text{-}fl/fl}$	QIMR Berghofer	
Mouse: *Tie2*-Cre *I-A*$^{b\text{-}fl/fl}$	QIMR Berghofer	
Mouse: *Villin*-Cre *Rosa26*-YFP	QIMR Berghofer	
Mouse: *Nestin*-Cre *Rosa26*-YFP	QIMR Berghofer	
Mouse: *Tie2*-Cre *Rosa26*-YFP	QIMR Berghofer	
Oligonucleotides		

REAGENT or RESOURCE	SOURCE	IDENTIFIER
NIA		
Recombinant DNA		
NIA		
Software and Algorithms		
BD FACSDiva software version 8	BD Bioscience	https://www.bdbiosciences.com/in/instruments/software/facsdiva/
FlowJo v9	Tree Star	https://www.flowjo.com/
Zen software	Zeiss	https://www.zeiss.com/microscopy/int/downloads/brochure-downloads.html?filter=en_de%7E00012806
ImageJ 1.51w	NIH	https://imagej.nih.gov/ij/docs/intro.html
Cutadapt	Marcel Martin, 2011 https://doi.org/10.14806/ej.17.1.200	https://github.com/marcelm/cutadapt
STAR	Doblin A et al., 2013 https://www.ncbi.nlm.nih.gov/pubmed/23104886	https://github.com/alexdobin/STAR
EdgeR	Robinson MD et al., 2010 Bioconductor 3.9	http://bioconductor.org/packages/release/bioc/html/edgeR.html
GSEA	Broad Institute	http://software.broadinstitute.org/gsea/index.jsp
GraphPad Prism (ver. 7.02)	GraphPad Software	https://www.graphpad.com/scientific-software/prism/
Other		
BD LSRFortessa	BD Bioscience	https://www.bdbiosciences.com/in/instruments/lsr/index.jsp
Xenogen IVIS 100	Caliper Life Sciences	https://www.perkinelmer.com/product/ivis-spectrum-imaging-system-120v-124262
Zeiss 780-NLO Point Scanning Confocal Microscope	Zeiss	https://www.zeiss.com/microscopy/int/service-support/glossary/nlo.html
Olympus BX51 microscope	Olympus	https://www.olympus-lifescience.com/en/microscope-resource/primer/java/lightpaths/bx51fluorescence/